CSIAM Trans. Life Sci.
doi: 10.4208/csiam-ls.SO-2025-0010

Vol. **x**, No. x, pp. 1-29
xx 2025

Modeling Effects of T Cell Exhaustion on the Dynamics of Chronic Viral Infection

Teng Yu and Xiulan Lai*

School of Mathematics, Renmin University of China, Beijing 100872, P.R. China.

Received 11 May 2025; Accepted 26 July 2025

Abstract. During chronic viral infection, sustained antigen stimulation leads to exhaustion of virus-specific $CD8^+$ T cells, characterized by elevated expression of inhibitory receptors and progressive functional impairment, including loss of cytokine production, reduced cytotoxicity, and diminished proliferative capacity. In this paper, to investigate how T cell exhaustion influences viral persistence, we developed a within-host mathematical model integrating viral infection dynamics with adaptive immune responses. The model demonstrates three non-trivial equilibria: infection-free equilibrium (S_1), uncontrolled-infection state (S_2), and immune-controlled equilibrium (S_3). Through dynamical systems analysis, we established the local stability of all states (S_1-S_3) and prove global stability for both S_1 (complete viral clearance) and S_2 (chronic infection). Notably, the system exhibits Hopf bifurcations at S_2 and S_3, with distinct critical thresholds governing oscillatory dynamics. Numerical simulations reveal that successful immune-mediated control of viral load and infected cell levels requires maintenance of low $CD8^+$ T cell exhaustion rates.

AMS subject classifications: Primary: 34K20, 92B05; Secondary: 34K25, 92D25

Key words: Viral infection dynamics, T cell exhaustion, stability analysis, Hopf bifurcation.

1 Introduction

The T-cell response plays a central role in the adaptive immune-mediated clearance of pathogen-infected cells. During acute infection, antigen-specific naive $CD8^+$ T cells undergo activation, clonal expansion, and effector differentiation following antigen recognition and costimulatory signaling [12]. While most effector cells are eliminated via apoptosis after pathogen clearance, a small subset persists to form the memory $CD8^+$ T cell compartment [13,14]. To ensure proper immune termination and maintain self-tolerance,

*Corresponding author. *Email address:* xiulanlai@ruc.edu.cn (X. Lai)

inhibitory receptors/immune checkpoint molecules are transiently upregulated on activated effector T cells during the resolution phase [30]. Following antigen clearance, expression of these regulatory molecules gradually returns to baseline levels in memory T cells. This tightly regulated process represents a critical self-limiting mechanism of adaptive immunity, balancing effective pathogen clearance with prevention of excessive immune activation.

In chronic infections, however, persistent antigen exposure of $CD8^+$ T cells to high levels of antigen drives T cells into a severe T-cell dysfunctional state called exhaustion [2, 11, 26, 36], first identified in murine lymphocytic choriomeningitis virus (LCMV) models and later observed in human chronic viral infections (e.g. human imunodeficiency virus (HIV), hepatitis B virus (HBV), hepatitis C virus (HCV)). Exhausted T cells (T_{ex}) exhibit progressive functional decline [9, 26], marked by: (i) impaired cytotoxicity, reduced cytokine production (e.g. IL-2, IFN-γ), and limited proliferative capacity; and (ii) upregulated co-inhibitory receptors (such as programmed cell death protein 1 (PD-1), cytotoxic T-lymphocyte-associated protein 4 (CTLA-4), T cell immunoglobulin and mucin domain containing-3 (TIM-3), lymphocyte activation gene 3 (LAG-3)), which further suppress T-cell function. This exhausted T cell compartment is developmentally distinct from conventional effector T cells and comprises heterogeneous subsets [4, 9, 39]: stem-like $CD8^+T_{ex}$ precursors/progenitors, effector-like transitory $CD8^+T_{ex}$, and terminally dysfunctional $CD8^+T_{ex}$. The stem-like $CD8^+$ T_{ex} precursors/progenitors exhibit proliferative potential but low inhibitory receptor expression, while effector-like transitory $CD8^+$ T_{ex} has high proliferative potential and transient cytotoxicity. In contrast, terminally dysfunctional $CD8^+T_{ex}$ cells exhibit multiple irreversible functional impairments, including restricted proliferative capacity, diminished cytotoxic activity, and elevated expression of multiple co-inhibitory receptors [29]. While stem-like $CD8^+T_{ex}$ sustain immune responses, terminal subsets are shown to dominate in high-antigen environments, perpetuating immune evasion [40].

Mathematical models have been extensively used to explore within-host chronic viral infection dynamics and the corresponding immune response and treatment strategies, including HIV [5, 10, 17, 18, 27, 31, 32, 37, 38, 41], HBV and HCV [7, 34, 43]. The basic model [5, 27] employs a three-compartment ODE framework (uninfected target cells, infected cells, and free virions) to comprehensively represent a within-host viral infection dynamics, The model's dynamical behavior is primarily governed by the basic reproduction number [18]. The basic model has been extended to incorporate: latent reservoirs [10, 43], cell-to-cell transmission [17, 19, 32], adaptive immune regulation [8, 35, 37, 38, 41], antiviral drug interventions [7, 31, 34], coupling of within-host and between-host dynamics [1]. These models have provided key insights for HIV, HBV/HCV, and other chronic infections.

Through analysis of HIV-immune system interactions during natural infection and under various treatment regimens, Wodarz and Nowak [41] demonstrated that sustained viral control depends critically on robust cytotoxic T lymphocyte (CTL) memory responses. Their mathematical modeling revealed that specific treatment schedule interruptions

could re-establish functional CTL memory. The possibility of reconstituting the CTL immune response through antiretroviral therapy is further confirmed by Wang *et al.* [38]. Through quantitative analysis of virus-T cell interactions, Davenport *et al.* [8] evaluated the efficacy of humoral and cell-mediated immune control, and showed the limitations of cytotoxic lymphocyte responses in preventing viral persistence.

In the previous work [20], we considered a viral infection model with virus-to-cell and cell-to-cell viral spread and logistic target cell growth, and identified the basic reproduction number and the dynamics of viral infection. In this paper, we extend the model in [20] to include the effects of $CD8^+$ T cell immune response and explore the influences of $CD8^+$ T cell exhaustion on viral dynamics. To simplify the exhaustion continuum while maintaining clinically meaningful functional distinctions, we adopt a two-tier classification system for $CD8^+$ T cell exhaustion. Stem-like precursors and effector-like transitory populations are grouped under a unified $CD8^+$ T designation, based on their shared functional properties and relatively low expression of inhibitory receptors despite transcriptional heterogeneity [4]. This classification distinguishes them from terminally exhausted $CD8^+$ T cells, which exhibit irreversible dysfunction and high expression of inhibitory receptors.

The model for viral infection and $CD8^+$ T cell response dynamics are given as follows:

$$\cdot\begin{cases} \dfrac{\mathrm{d}T(t)}{\mathrm{d}t} = r_1 T(t)\left(1-\dfrac{T(t)}{T_M}\right) - \beta_1 T(t)V(t) - \beta_2 T(t)I(t), \\ \dfrac{\mathrm{d}I(t)}{\mathrm{d}t} = \beta_1 T(t)V(t) + \beta_2 T(t)I(t) - \alpha I(t)E(t) - d_I I(t), \\ \dfrac{\mathrm{d}V(t)}{\mathrm{d}t} = \gamma I(t) - d_V V(t), \\ \dfrac{\mathrm{d}E(t)}{\mathrm{d}t} = r_2 E(t)I(t) - \rho E(t)I(t) - d_E E(t), \\ \dfrac{\mathrm{d}E^*(t)}{\mathrm{d}t} = \rho E(t)I(t) - d_{E^*} E^*(t). \end{cases} \tag{1.1}$$

Here, $T(t), I(t)$ and $V(t)$ represent the concentrations of susceptible/target cells, productively infected cells, and free viral particles at time t, respectively; $E(t)$ and $E^*(t)$ denote the concentrations of $CD8^+$ T cells and exhausted $CD8^+$ T cells, respectively. In the model, susceptible cells are assumed to follow a logistic growth, and are infected by free viruses and cell-to-cell viral spread at rates of $\beta_1 T(t)V(t)$ and $\beta_2 T(t)V(t)$, respectively. The parameter r_1 represents the baseline growth rate of target cells; T_M denotes the carrying capacity. Productively infected cells die at a rate $d_I I(t)$ and eliminated by $CD8^+$ T cells at a rate $\alpha I(t)E(t)$. Free viral particles are released from infected cells at a rate of $\gamma I(t)$ and cleared at a rate $d_V V(t)$. $CD8^+$ T cells are activated to grow with viral-antigen presentation at a rate $r_2 E(t)I(t)$, and exhaust under chronic antigen stimulation at a rate $\rho E(t)I(t)$. The $CD8^+$ T cells and exhausted $CD8^+$ T cells undergo apoptosis at rates $d_E E(t)$ and $d_{E^*} E^*(t)$, respectively.

For mathematical convenience, we rescale the system (1.1) by

$$u(t)=\frac{T(t)}{T_M},\quad w(t)=\frac{I(t)}{T_M},\quad v(t)=\frac{d_I}{\gamma T_M}V(t),\quad x(t)=\frac{E(t)}{E_M},\quad y(t)=\frac{E^*(t)}{E_M},$$
$$\tilde{t}=d_I t,\qquad \delta_1=\frac{r_1}{d_I},\qquad \rho_1=\frac{\beta_1\gamma T_M}{d_I^2},\qquad \rho_2=\frac{\beta_2 T_M}{d_I},\quad \rho_3=\frac{\alpha}{d_I}E_M,$$
$$\delta_2=\frac{r_2 T_M}{d_I},\quad \mu_1=\frac{d_V}{d_I},\quad \mu_2=\frac{d_E}{d_I},\quad \mu_3=\frac{d_{E^*}}{d_I},\quad \eta=\frac{\rho T_M}{d_I},$$

and obtain the non-dimensionalized model

$$\begin{cases}\dfrac{\mathrm{d}u(t)}{\mathrm{d}t}=\delta_1 u(t)[1-u(t)]-\rho_1 u(t)v(t)-\rho_2 u(t)w(t), & (1.2a)\\ \dfrac{\mathrm{d}w(t)}{\mathrm{d}t}=\rho_1 u(t)v(t)+\rho_2 u(t)w(t)-w(t)-\rho_3 x(t)w(t), & (1.2b)\\ \dfrac{\mathrm{d}v(t)}{\mathrm{d}t}=w(t)-\mu_1 v(t), & (1.2c)\\ \dfrac{\mathrm{d}x(t)}{\mathrm{d}t}=\delta_2 x(t)w(t)-\eta x(t)w(t)-\mu_2 x(t), & (1.2d)\\ \dfrac{\mathrm{d}y(t)}{\mathrm{d}t}=\eta x(t)w(t)-\mu_3 y(t). & (1.2e)\end{cases}$$

Applying this model, we investigate the effects of T cell exhaustion on the viral dynamics. The rest of the paper is organized as follows. Nonnegativity and boundedness of the solutions, and the existence and local/global stability of the equilibrium of the model are shown in Section 2. Numerical simulation about the bifurcation of the system and the effects of T cell exhaustion are demonstrated in Section 3. Conclusion and discussion are presented in Section 4.

2 Stability analysis

2.1 Nonnegativity and boundedness of solutions

Theorem 2.1. *System* (1.2) *admits a unique solution for any initial condition* $(u_0,w_0,v_0,x_0,y_0)\in\mathbb{X}$, *where the state space* $\mathbb{X}$ *and its interior* $\mathbb{X}_0$ *are positively invariant under the solution semiflow. Specifically, these sets are defined as*

$$\mathbb{X}:=\left\{(u,w,v,x,y)\in\mathbb{R}^5\,\middle|\,u,w,v,x,y\geq 0,u+w\leq 1,\frac{\delta_2-\eta}{\rho_3}w+x\leq\zeta,v\leq\frac{1}{\mu_1},y\leq\frac{\eta\zeta}{\mu_3}\right\},$$
$$\mathbb{X}_0:=\{(u,w,v,x,y)\in\mathbb{X}\,|\,u>0,w>0,v>0,x>0,y>0\},$$

where

$$\zeta:=\frac{\delta_2-\eta}{\rho_3}\left(\frac{\rho_1}{\mu_1}+\rho_2\right)\max\left\{\frac{1}{\mu_2},1\right\}.$$

Proof. The right-hand side functions of (1.2) satisfy Lipschitz condition, ensuring the existence and uniqueness of a solution $(u(t),w(t),v(t),x(t),y(t)) \in C([0,+\infty),\mathbb{R}_+)$ to system (1.2) for any initial condition $(u_0,w_0,v_0,x_0,y_0) \in \mathbb{X}$. Moreover, the solution admits the following representation:

$$
\begin{aligned}
&u(t) = u_0 \exp\left\{\int_0^t \left[\delta_1\left(1-u(s)\right) - \rho_1 v(s) - \rho_2 w(s)\right] ds\right\} \geq 0,\\
&x(t) = x_0 \exp\left\{\int_0^t \left[\delta_2 w(s) - \eta w(s) - \mu_2\right] ds\right\} \geq 0,\\
&w(t) = \mathrm{e}^{\int_0^t f(\tau)\mathrm{d}\tau}\left(w_0 + \int_0^t \mathrm{e}^{\int_0^s f(\tau)\mathrm{d}\tau} u(s)v(s)\mathrm{d}s\right), \quad f(t) := \rho_2 u(t) - 1 - \rho_3 x(t),\\
&v(t) = \mathrm{e}^{-\mu_1 t}\left(v_0 + \int_0^t \mathrm{e}^{-\mu_1 s} w(s)\mathrm{d}s\right),\\
&y(t) = \mathrm{e}^{-\mu_3 t}\left(y_0 + \int_0^t \mathrm{e}^{-\mu_3 s} x(s)w(s)\mathrm{d}s\right), \quad t \geq 0.
\end{aligned}
$$

Note that $(u,w,v,x,y) = (0,0,0,0,0)$ is a solution to the system (1.2). If $u(0) = u_0 = 0$, then $u(t) \equiv 0$, for $t \geq 0$, and $w(t) = w_0 \mathrm{e}^{\int_0^t f(\tau)\mathrm{d}\tau} \geq 0, v(t) \geq 0$ and $y(t) \geq 0$ for $t \geq 0$. In the following, we assume $u(0) = u_0 > 0$, so that $u(t) > 0$ for $t > 0$.

From the equations of w and v in (1.2), we observe that $w(t)$ and $v(t)$ are either both identically zero or both non-zero for all $t > 0$. If $w(t) \equiv 0$ and $v(t) \equiv 0$, then $y(t) = y_0 \mathrm{e}^{-\mu_3 t} \geq 0$ for $t \geq 0$. When $w(t)$ and $v(t)$ are not identically zero (requiring $w_0 > 0$ or $v_0 > 0$), we show both remain positive for $t > 0$. Suppose for contradiction that $w(t_1) = 0$ for some $t_1 > 0$ while $w(t) > 0$ for $t \in [0,t_1)$, then

$$
v(t) = \mathrm{e}^{-\mu_1 t}\left(v_0 + \int_0^t \mathrm{e}^{-\mu_1 s} w(s)\mathrm{d}\right) > 0, \quad 0 < t < t_1,
$$

implying

$$
w(t_1) = \mathrm{e}^{\int_0^{t_1} f(\tau)\mathrm{d}\tau}\left(w_0 + \int_0^{t_1} \mathrm{e}^{\int_0^s f(\tau)\mathrm{d}\tau} u(s)v(s)\mathrm{d}s\right) > 0,
$$

a contradiction. Similarly, assuming $v(t_2) = 0$ at $t_2 > 0$ with $v(t) > 0$ on $[0,t_2)$ forces $w(t) > 0$ on $(0,< t_2)$, making $v(t_2) > 0$, again a contradiction. Thus, $w(t) > 0$ and $v(t) > 0$ for all $t > 0$, when $w_0 > 0$ or $v_0 > 0$, and consequently, $w(t) \geq 0$ and $v(t) \geq 0$, for $t \geq 0$, furthermore, $y(t) \geq 0$ for $t \geq 0$.

If $u(0) = u_0 > 0$, $w(0) = w_0 > 0$, $v(0) = v_0 > 0$, $x(0) = x_0 > 0$ and $y(0) = y_0 > 0$, then $u(t) > 0$ and $x(t) > 0$. Additionally, from Eqs. (1.2b) and (1.2c), we have

$$
\frac{\mathrm{d}w}{\mathrm{d}t} \geq \rho_2 u(t)w(t) - w(t) - \rho_3 x(t)w(t), \quad \frac{\mathrm{d}v}{\mathrm{d}t} \geq -\mu_1 v.
$$

By a comparison argument, it follows that

$$w(t) \geq w_0 \exp\left\{\int_0^t [\rho_2 u(s) - 1 - \rho_3 x(s)] ds\right\} > 0,$$
$$v(t) \geq v_0 e^{-\mu_1 t} > 0$$

for $t \geq 0$, as $w_0 > 0$ and $v_0 > 0$. Similarly, we also obtain that $y(t) \geq y_0 e^{-\mu_3 t} > 0$ for $t \geq 0$.

Next, with the non-negativity of solutions, we prove they are bounded. For $u(t)+w(t)$,

$$\begin{aligned}\frac{\mathrm{d}}{\mathrm{d}t}[u(t)+w(t)] &= \delta_1 u(t)[1-u(t)] - w(t) - \rho_3 x(t) w(t) \\ &\leq \delta_1 u(t)[1-u(t)].\end{aligned}$$

By a comparison argument, we see that $u(t)+w(t) \leq \max\{u_0, 1\}$ for $t \geq 0$. Thus, we have $u(t) < 1$ and $w(t) < 1$ for $t \geq 0$. From the Eq. (1.2c),

$$\frac{\mathrm{d}v(t)}{\mathrm{d}t} = w(t) - \mu_1 v(t) \leq 1 - \mu_1 v(t),$$

which implies

$$v(t) \leq e^{-\mu_1 t}\left(v_0 - \frac{1}{\mu_1}\right) + \frac{1}{\mu_1} \leq \frac{1}{\mu_1}$$

for $v_0 \leq 1/\mu_1, t \geq 0$. From the Eq. (1.2d),

$$x(t) = x_0 \exp\left\{\int_0^t [\delta_2 w(s) - \eta w(s) - \mu_2] ds\right\}.$$

If $\delta_2 - \eta - \mu_2 \leq 0$, then $x(t) \leq x_0 e^{-\mu_2 t} \leq x_0$. When $\delta_2 - \eta - \mu_2 > 0$, notice that

$$\frac{\mathrm{d}}{\mathrm{d}t}\left[\frac{\delta_2-\eta}{\rho_3} w(t) + x(t)\right] = \frac{\delta_2-\eta}{\rho_3}[\rho_1 u(t) v(t) + \rho_2 u(t) w(t) - w(t)] - \mu_2 x(t),$$

we have

$$\begin{aligned}&\frac{\mathrm{d}}{\mathrm{d}t}\left[\frac{\delta_2-\eta}{\rho_3} w(t) + x(t)\right] \leq \frac{\delta_2-\eta}{\rho_3}\left(\frac{\rho_1}{\mu_1} + \rho_2\right) - \mu_2\left[\frac{\delta_2-\eta}{\rho_3} w(t) + x(t)\right] x(t), \quad \mu_2 \leq 1, \\ &\frac{\mathrm{d}}{\mathrm{d}t}\left[\frac{\delta_2-\eta}{\rho_3} w(t) + x(t)\right] \leq \frac{\delta_2-\eta}{\rho_3}\left(\frac{\rho_1}{\mu_1} + \rho_2\right) - \left[\frac{\delta_2-\eta}{\rho_3} w(t) + x(t)\right] x(t), \qquad \mu_2 > 1.\end{aligned}$$

Let

$$\zeta := \frac{\delta_2-\eta}{\rho_3}\left(\frac{\rho_1}{\mu_1} + \rho_2\right) \max\left\{\frac{1}{\mu_2}, 1\right\},$$

then with a similar argument as proof of $v(t)$ boundedness, it holds that

$$\frac{\delta_2-\eta}{\rho_3} w(t) + x(t) \leq \zeta, \quad \text{if} \quad \frac{\delta_2-\eta}{\rho_3} w_0 + x_0 \leq \zeta.$$

From the Eq. (1.2e),

$$\frac{\mathrm{d}y(t)}{\mathrm{d}t}=\eta x(t)w(t)-\mu_3 y(t)\leq \eta\zeta-\mu_3 y(t),$$

which implies that $y(t)\leq \eta\zeta/\mu_3$, if $y_0\leq \eta\zeta/\mu_3$.

In summary, the sets $\mathbb{X}$ and $\mathbb{X}_0$ are positively invariant for the semiflow of the system (1.2). □

2.2 Local stability analysis

For model (1.2), there exist two critical thresholds governing viral infection and immune response establishment. The basic reproduction number of the virus is given by

$$\mathcal{R}_0=\frac{\rho_1}{\mu_1}+\rho_2.$$

The threshold for immune response establishment is given by

$$\mathcal{R}_1=\frac{\delta_2-\eta}{\mu_2}\frac{\delta_1}{\mathcal{R}_0}\left(1-\frac{1}{\mathcal{R}_0}\right).$$

We assume that $\delta_2>\eta$ in all follows. There exist four possible equilibria for the system (1.2), which are given by the following lemma. To investigate bifurcation of the system, we denote the parameters involved in the model as $p, p:=(\delta_1,\rho_1\rho_2,\rho_3,\mu_1,\delta,\eta,\mu_2)$.

Lemma 2.1. *For system* (1.2)*, the following holds:*

(i) The trivial equilibrium $S_0=(0,0,0,0,0)$ and the infection-free equilibrium $S_1=(1,0,0,0,0)$ always exist.

(ii) If $\mathcal{R}_0>1$, it has an uncontrolled-infection equilibrium $S_2=(\bar{u},\bar{w},\bar{v},0,0)$, where

$$\bar{u}=\frac{1}{\mathcal{R}_0},\quad \bar{w}=\frac{\delta_1}{\mathcal{R}_0}\left(1-\frac{1}{\mathcal{R}_0}\right),\quad \bar{v}=\frac{\bar{w}}{\mu_1}.$$

(iii) If $\mathcal{R}_0>1$ and $\mathcal{R}_1>1$, it has an immune-controlled equilibrium $S_4=(\hat{u},\hat{w},\hat{v},\hat{x},\hat{y})$, where

$$\hat{u}=1-\frac{\mathcal{R}_0-1}{\mathcal{R}_0\mathcal{R}_1},\quad \hat{w}=\frac{\mu_2}{\delta_2-\eta},\quad \hat{v}=\frac{\hat{w}}{\mu_1},\quad \hat{x}=\frac{(\mathcal{R}_0-1)(\mathcal{R}_1-1)}{\rho_3\mathcal{R}_1},\quad \hat{y}=\frac{\eta\hat{x}\hat{w}}{\mu_3}.$$

Note here that $\hat{w}=\bar{w}/\mathcal{R}_1$ and $\hat{v}=\bar{w}/\mu_1\mathcal{R}_1$, thus $\hat{w}<\bar{w}$, as $\mathcal{R}_1>1$.

The equilibria $S_i, i=1,2,3$, are locally asymptotically stable (LAS), under different conditions, respectively, which are shown in the following theorems. The Jacobian matrix of system (1.2) at an equilibrium (u,w,v,x,y) is given by

$$J=\begin{pmatrix}
\delta_1(1-2u)-\rho_1 v-\rho_2 w & -\rho_2 u & -\rho_1 u & 0 & 0\\
\rho_1 v+\rho_2 w & \rho_2 u-\rho_3 x-1 & \rho_1 u & -\rho_3 w & 0\\
0 & 1 & -\mu_1 & 0 & 0\\
0 & \delta_2 x-\eta x & 0 & \delta_2 w-\eta w-\mu_2 & 0\\
0 & \eta x & 0 & \eta w & -\mu_3
\end{pmatrix}.$$

The stability conditions for $S_1=(1,0,0,0,0)$ and $S_2=(\bar{u},\bar{w},\bar{v},0,0)$ are the same as those in [20], which are shown in the following theorem.

Theorem 2.2. *For system* (1.2)*, the following holds:*

(i) The trivial equilibrium $S_0=(0,0,0,0,0)$ is always unstable.

(ii) If $\mathcal{R}_0<1$, the infection-free equilibrium $S_1=(1,0,0,0,0)$ is LAS. If $\mathcal{R}_0>1$, $S_1=(1,0,0,0,0)$ is unstable.

(iii) If $\mathcal{R}_0=1$, S_1 is nonhyperbolic, and the system experiences a transcritical bifurcation at S_1 as the parameter p passes through the bifurcation value $p=p_0$ which satisfies $\mathcal{R}_0=1$.

(iv) If $\mathcal{R}_0>1>\mathcal{R}_1$ and $\phi_1(p)>0$, the uncontrolled-infection equilibrium $S_2=(\bar{u},\bar{w},\bar{v},0,0)$ is LAS. If $\mathcal{R}_1>1$ or $\phi_1(p)<0$, $S_2=(\bar{u},\bar{w},\bar{v},0,0)$ is unstable (assuming $\mathcal{R}_0>1$).

(v) Assuming $\mathcal{R}_0>1$, $\mathcal{R}_1\neq 1$, the system has a Hopf bifurcation at S_2 if and only if $\phi_1(p)=0$. Here, the formula of $\phi_1(p)$ is given by (2.1) *in the following proof.*

Proof. (i)-(iii) The Jacobian matrix of system (1.2) at S_0 and S_1 are given by

$$J(S_0)=\begin{pmatrix}\delta_1 & 0 & 0 & 0 & 0\\ 0 & -1 & 0 & 0 & 0\\ 0 & 1 & -\mu_1 & 0 & 0\\ 0 & 0 & 0 & -\mu_2 & 0\\ 0 & 0 & 0 & 0 & -\mu_3\end{pmatrix},\quad J(S_1)=\begin{pmatrix}-\delta_1 & -\rho_2 & -\rho_1 & 0 & 0\\ 0 & \rho_2-1 & \rho_1 & 0 & 0\\ 0 & 1 & -\mu_1 & 0 & 0\\ 0 & 0 & 0 & -\mu_2 & 0\\ 0 & 0 & 0 & 0 & -\mu_3\end{pmatrix},$$

respectively. Since $J(S_0)$ has a positive eigenvalue $\lambda=\delta_1$, E_0 is always unstable. $J(S_1)$ has three eigenvalues $\lambda_1=-\delta_1<0, \lambda_4=-\mu_2<0, \lambda_5=-\mu_3<0$, and other eigenvalues are given by the characteristic equation

$$\lambda^2+a_1\lambda+a_2=0,$$

where

$$a_1=\mu_1+1-\rho_2,\quad a_2=\mu_1(1-\rho_2)-\rho_1=\mu_1(1-\mathcal{R}_0).$$

We see that if $\mathcal{R}_0<1$, then $a_1>0, a_2>0$, and all eigenvalues of $J(S_1)$ have negative real parts, so that S_1 is LAS. If $\mathcal{R}_0>1$, then $a_2<0$, and J_{10} has at least one eigenvalue with positive real part so that S_1 is unstable.

If $\mathcal{R}_0=1$, then $a_1>0, a_2=0$, and J_{10} has one zero eigenvalue $\lambda=0$, thus S_1 is nonhyperbolic. Without loss of generality, we set ρ_1 as a bifurcation parameter, and employ Sotomayor's theorem [28, Theorem 4.2.1] to show that a transcritical bifurcation occurs at S_1 when ρ_1 passes through the critical value $\rho_1^c=(1-\rho_2)\mu_1$ for $\mathcal{R}_0=1$, assuming $\rho_2<1$. The right and left eigenvectors of the Jacobian matrix $J(S_1)$ with respect to the eigenvalue $\lambda=0$ is $U=(-\mu_1/\delta_1,\mu_1,1,0,0)^\top$ and $U^*=(0,\mu_1/\rho_1,1,0,0)$, respectively. Denoting the right-hand side of system (1.2) as $\mathbf{f}(u,w,v,x,y)$, we obtain by a general calculation that $\mathbf{f}_{\rho_1}=(-uv,uv,0,0,0)^\top$, and

$$(U^*)^\top\mathbf{f}_{\rho_1}\left(S_1,\rho_1^c\right)=0,$$

$$(U^*)^\top\left[D\mathbf{f}_{\rho_1}(S_1,\rho_1^c)U\right]=-\frac{\mu_1}{\rho_1^c}\neq 0,$$
$$(U^*)^\top\left[D^2\mathbf{f}_{\rho_1}(S_1,\rho_1^c)(U,U)\right]=-\frac{\mu_1^3}{\delta_1}\left(\frac{1}{\rho_1^c}+\frac{1}{\mu_1}+1\right)\neq 0.$$

By Sotomayor's theorem [28, Theorem 4.2.1], system (1.2) undergoes a transcritical bifurcation at S_1 when ρ_1 passes the critical value ρ_1^c.

(iv)-(v) The Jacobian matrix of system (1.2) at $S_2=(\bar{u},\bar{w},\bar{v},0,0)$ is given by

$$J(S_2)=\begin{pmatrix} -\frac{\delta_1}{\mathcal{R}_0} & -\frac{\rho_2}{\mathcal{R}_0} & -\frac{\rho_1}{\mathcal{R}_0} & 0 & 0\\ \frac{\delta_1(\mathcal{R}_0-1)}{\mathcal{R}_0} & \frac{\rho_2}{\mathcal{R}_0}-1 & \frac{\rho_1}{\mathcal{R}_0} & -\rho_3\bar{w} & 0\\ 0 & 1 & -\mu_1 & 0 & 0\\ 0 & 0 & 0 & \delta_2\bar{w}-\eta\bar{w}-\mu_2 & 0\\ 0 & 0 & 0 & \eta\bar{w} & -\mu_3 \end{pmatrix}.$$

It has two eigenvalues $\lambda_5=-\mu_3<0$, and $\lambda_4=\delta_2\bar{w}-\eta\bar{w}-\mu_2$, where $\lambda_4<0$ if $\mathcal{R}_1<1$. The other eigenvalues of $J(S_2)$ are given by the roots of characteristic equation

$$\lambda^3+a_1\lambda^2+a_2\lambda+a_3=0,$$

where

$$a_1=\frac{\delta_1}{\mathcal{R}_0}+\mu_1+\frac{\rho_1}{\mu_1\mathcal{R}_0}>0,$$
$$a_2=\frac{\delta_1}{\mathcal{R}_0}\left(\mu_1+\frac{\rho_1}{\mu_1\mathcal{R}_0}+\frac{\rho_2}{\mathcal{R}_0}(\mathcal{R}_0-1)\right),$$
$$a_3=\frac{\delta_1\mu_1}{\mathcal{R}_0}(\mathcal{R}_0-1).$$

Note that $a_2>0, a_3>0$ as $\mathcal{R}_0>1$. In addition, if $a_1a_2-a_3>0$, the equilibrium S_2 is LAS by the Routh–Hurwitz criterion, where

$$\begin{aligned} &a_1a_2-a_3\\ &=\frac{\delta_1}{\mathcal{R}_0}\left\{\left(\frac{\delta_1}{\mathcal{R}_0}+\mu_1+\frac{\rho_1}{\mu_1\mathcal{R}_0}\right)\left(\mu_1+\frac{\rho_1}{\mu_1\mathcal{R}_0}\right)+(\mathcal{R}_0-1)\left[\left(\frac{\delta_1}{\mathcal{R}_0}+\mu_1+\frac{\rho_1}{\mu_1\mathcal{R}_0}\right)\frac{\rho_2}{\mathcal{R}_0}-\mu_1\right]\right\}\\ &=\frac{\delta_1}{\mathcal{R}_0}\left\{\left(\frac{\delta_1}{\mathcal{R}_0}+\mu_1+\frac{\rho_1}{\mu_1\mathcal{R}_0}\right)\left[\left(\mu_1+\frac{\rho_1}{\mu_1\mathcal{R}_0}\right)+(\mathcal{R}_0-1)\frac{\rho_2}{\mathcal{R}_0}\right]-(\mathcal{R}_0-1)\mu_1\right\}. \end{aligned}$$

Let

$$\phi_1(p):=\left(\frac{\delta_1}{\mathcal{R}_0}+\mu_1+\frac{\rho_1}{\mu_1\mathcal{R}_0}\right)\left[\left(\mu_1+\frac{\rho_1}{\mu_1\mathcal{R}_0}\right)+(\mathcal{R}_0-1)\frac{\rho_2}{\mathcal{R}_0}\right]-(\mathcal{R}_0-1)\mu_1, \tag{2.1}$$

where $p=(\delta_1,\rho_1,\rho_2,\mu_1)$. We see that equilibrium S_2 is LAS, if $\mathcal{R}_0>1$ and $\phi_1(p)>0$.

On the other hand, if $\mathcal{R}_1>1$ or $\phi_1(p)<0$, then $J(S_2)$ has eigenvalue with positive real parts ($\lambda_4>0$ or one/two of $\lambda_i, i=1,2,3$), implying that S_2 is unstable. By [42], the necessary and sufficient condition for system (1.2) to have a Hopf bifurcation at S_2 is $\phi_1(p)=0$, assuming $\mathcal{R}_0>1$ and $\mathcal{R}_1\neq 1$, thereby $J(S_2)$ has a pair of pure imaginary eigenvalues $\lambda=\pm i\sqrt{a_2}$. □

Remark 2.1. Notice that if

$$\left(\frac{\delta_1}{\mathcal{R}_0}+\mu_1+\frac{\rho_1}{\mu_1\mathcal{R}_0}\right)\frac{\rho_2}{\mathcal{R}_0}>\mu_1,$$

that is,

$$\delta_1>\rho_2+\left(\frac{\rho_1}{\rho_2}-1\right)\mathcal{R}_0,$$

then $a_1a_2-a_3>0$. Thus, if $\mathcal{R}_0>1>\mathcal{R}_1$, and

$$\left(\frac{\delta_1}{\mathcal{R}_0}+\mu_1+\frac{\rho_1}{\mu_1\mathcal{R}_0}\right)\frac{\rho_2}{\mathcal{R}_0}>\mu_1,$$

then the equilibrium S_2 is LAS.

For the stability of the immune-controlled equilibrium S_3, we have the following results.

Theorem 2.3. *For system* (1.2)*, with* $\mathcal{R}_0>1, \mathcal{R}_1>1$*, we have:*

(i) If $\phi_2(p)>0$ *and* $\phi_3(p)>0$*, the immune-controlled equilibrium* $S_3=(\hat{u},\hat{w},\hat{v},\hat{x},\hat{y})$ *is LAS.*

(ii) If $\phi_2(p)<0$ *or* $\phi_3(p)<0$*, then* $S_3=(\hat{u},\hat{w},\hat{v},\hat{x},\hat{y})$ *is unstable.*

(iii) The system has a Hopf bifurcation at S_2 *if and only if* $\phi_3(p)=0$*.*

Here, the formulas of $\phi_2(p)$ *and* $\phi_3(p)$ *are given by* (2.2) *and* (2.3)*, respectively.*

Proof. The Jacobian matrix of system (1.2) at $S_3=(\hat{u},\hat{w},\hat{v},\hat{x},\hat{y})$ is given by

$$J(S_3)=\begin{pmatrix} -\delta_1\hat{u} & -\rho_2\hat{u} & -\rho_1\hat{u} & 0 & 0\\ \dfrac{\mathcal{R}_0\bar{w}}{\mathcal{R}_1} & (\rho_2-\mathcal{R}_0)\hat{u} & \rho_1\hat{u} & -\dfrac{\rho_3\bar{w}}{\mathcal{R}_1} & 0\\ 0 & 1 & -\mu_1 & 0 & 0\\ 0 & \delta_2\hat{x}-\eta\hat{x} & 0 & 0 & 0\\ 0 & \eta\hat{x} & 0 & \eta\bar{w} & -\mu_3 \end{pmatrix},$$

which has an eigenvalue $\lambda_5=-\mu_3<0$, and other eigenvalues are given by the matrix

$$J_1(S_3)=\begin{pmatrix} -\delta_1\hat{u} & -\rho_2\hat{u} & -\rho_1\hat{u} & 0\\ \dfrac{\mathcal{R}_0\bar{w}}{\mathcal{R}_1} & (\rho_2-\mathcal{R}_0)\hat{u} & \rho_1\hat{u} & -\dfrac{\rho_3\bar{w}}{\mathcal{R}_1}\\ 0 & 1 & -\mu_1 & 0\\ 0 & \delta_2\hat{x}-\eta\hat{x} & 0 & 0 \end{pmatrix}.$$

The characteristic equation of $J_1(S_3)$ reads

$$\lambda^4+b_1\lambda^3+b_2\lambda^2+b_3\lambda+b_4=0,$$

where

$$\begin{aligned}
b_1&=\mathcal{R}_0\hat{u}-\rho_2\hat{u}+\delta_1\hat{u}+\mu_1=\frac{\rho_1}{\mu_1}\hat{u}+\delta_1\hat{u}+\mu_1>0,\\
b_2&=\frac{-\eta\bar{w}\hat{x}\rho_3+\bar{w}\hat{x}\delta_2\rho_3+\hat{u}\bar{w}\mathcal{R}_0\rho_2}{\mathcal{R}_1}+\hat{u}^2\delta_1\mathcal{R}_0-\hat{u}^2\delta_1\rho_2+\hat{u}\mathcal{R}_0\mu_1+\hat{u}\delta_1\mu_1-\hat{u}\mu_1\rho_2-\rho_1\hat{u}\\
&=\frac{\mathcal{R}_0\rho_2\hat{u}\bar{w}}{\mathcal{R}_1}+\mu_2\rho_3\hat{x}+\delta_1\frac{\rho_1}{\mu_1}\hat{u}^2+\delta_1\mu_1\hat{u}>0,\\
b_3&=\frac{\hat{u}\bar{w}\mathcal{R}_0(\mu_1\rho_2+\rho_1)+\rho_3\hat{x}(\hat{u}\delta_1+\mu_1)\bar{w}(\delta_2-\eta)}{\mathcal{R}_1}+\hat{u}^2\delta_1(\mathcal{R}_0\mu_1-\mu_1\rho_2-\rho_1)\\
&=\frac{\mu_1\mathcal{R}_0^2\hat{u}\bar{w}}{\mathcal{R}_1}+\mu_2\rho_3\hat{x}(\delta_1\hat{u}+\mu_1)>0,\\
b_4&=\frac{\hat{u}\hat{x}\delta_1\mu_1\rho_3\bar{w}(\delta_2-\eta)}{\mathcal{R}_1}=\delta_1\mu_1\mu_2\rho_3\hat{x}\hat{u}>0.
\end{aligned}$$

Therefore, if $b_1b_2-b_3>0$ and $b_3(b_1b_2-b_3)-b_1^2b_4>0$, then the equilibrium S_3 is LAS by the Routh-Hurwitz criterion, where

$$\begin{aligned}
b_1b_2-b_3&=\left(\frac{\rho_1}{\mu_1}\hat{u}+\delta_1\hat{u}+\mu_1\right)\left[\frac{\mathcal{R}_0\rho_2\hat{u}\bar{w}}{\mathcal{R}_1}+\mu_2\rho_3\hat{x}+\delta_1\frac{\rho_1}{\mu_1}\hat{u}^2+\delta_1\mu_1\hat{u}\right]\\
&\quad-\left[\frac{\mathcal{R}_0^2\mu_1\hat{u}\bar{w}}{\mathcal{R}_1}+\mu_2\rho_3\hat{x}(\delta_1\hat{u}+\mu_1)\right]\\
&=\left\{\frac{\rho_1}{\mu_1}\mu_2\rho_3\hat{x}+\left(\frac{\rho_1}{\mu_1}\hat{u}+\mu_1+\delta_1\hat{u}\right)\left(\frac{\rho_1}{\mu_1}\hat{u}+\mu_1\right)\delta_1+\left[\left(\frac{\rho_1}{\mu_1}+\delta_1\right)\rho_2\hat{u}-\rho_1\right]\frac{\mathcal{R}_0\bar{w}}{\mathcal{R}_1}\right\}\hat{u},
\end{aligned}$$

and

$$\begin{aligned}
&b_3(b_1b_2-b_3)-b_1^2b_4\\
&=\left\{\frac{\rho_1}{\mu_1}\mu_2\rho_3\hat{x}+\left(\frac{\rho_1}{\mu_1}\hat{u}+\mu_1+\delta_1\hat{u}\right)\left(\frac{\rho_1}{\mu_1}\hat{u}+\mu_1\right)\delta_1+\left[\left(\frac{\rho_1}{\mu_1}+\delta_1\right)\rho_2\hat{u}-\rho_1\right]\frac{\mathcal{R}_0\bar{w}}{\mathcal{R}_1}\right\}\hat{u}\\
&\quad\times\left[\frac{\mathcal{R}_0^2\mu_1\hat{u}\bar{w}}{\mathcal{R}_1}+\mu_2\rho_3\hat{x}(\delta_1\hat{u}+\mu_1)\right]-\delta_1\mu_1\mu_2\rho_3\hat{x}\hat{u}\left(\frac{\rho_1}{\mu_1}\hat{u}+\mu_1+\delta_1\hat{u}\right)^2\\
&=\left\{\mathcal{R}_0^2\mu_1\hat{u}\bar{w}\left[\frac{\rho_1}{\mu_1}\mu_2\rho_3\hat{x}+\left(\frac{\rho_1}{\mu_1}\hat{u}+\mu_1+\delta_1\hat{u}\right)\left(\frac{\rho_1}{\mu_1}\hat{u}+\mu_1\right)\delta_1\right]\right.\\
&\quad+\left[\mathcal{R}_0^2\mu_1\hat{u}\bar{w}+\mu_2\rho_3\hat{x}\mathcal{R}_1(\delta_1\hat{u}+\mu_1)\right]\left[\left(\frac{\rho_1}{\mu_1}+\delta_1\right)\rho_2\hat{u}-\rho_1\right]\frac{\mathcal{R}_0\bar{w}}{\mathcal{R}_1}\\
&\quad\left.+\frac{\rho_1}{\mu_1}\mu_2\rho_3\hat{x}\mathcal{R}_1\left[\frac{\rho_1}{\mu_1}\delta_1^2\hat{u}^3+(\delta_1^2\hat{u}^2+\mu_2\rho_3\hat{x})(\delta_1\hat{u}+\mu_1)\right]\right\}\frac{\hat{u}}{\mathcal{R}_1^2}.
\end{aligned}$$

Let

$$\phi_2(p) := \frac{\rho_1}{\mu_1}\mu_2\rho_3\hat{x} + \left(\frac{\rho_1}{\mu_1}\hat{u} + \mu_1 + \delta_1\hat{u}\right)\left(\frac{\rho_1}{\mu_1}\hat{u} + \mu_1\right)\delta_1 + \left[\left(\frac{\rho_1}{\mu_1} + \delta_1\right)\rho_2\hat{u} - \rho_1\right]\frac{\mathcal{R}_0\bar{w}}{\mathcal{R}_1}, \quad (2.2)$$

$$\begin{aligned}\phi_3(p) := {} & \mathcal{R}_0^2\mu_1\hat{u}\bar{w}\left[\frac{\rho_1}{\mu_1}\mu_2\rho_3\hat{x} + \left(\frac{\rho_1}{\mu_1}\hat{u} + \mu_1 + \delta_1\hat{u}\right)\left(\frac{\rho_1}{\mu_1}\hat{u} + \mu_1\right)\delta_1\right] \\ & + \left[\mathcal{R}_0^2\mu_1\hat{u}\bar{w} + \mu_2\rho_3\hat{x}\mathcal{R}_1(\delta_1\hat{u} + \mu_1)\right]\left[\left(\frac{\rho_1}{\mu_1} + \delta_1\right)\rho_2\hat{u} - \rho_1\right]\frac{\mathcal{R}_0\bar{w}}{\mathcal{R}_1} \\ & + \frac{\rho_1}{\mu_1}\mu_2\rho_3\hat{x}\mathcal{R}_1\left[\frac{\rho_1}{\mu_1}\delta_1^2\hat{u}^3 + \left(\delta_1^2\hat{u}^2 + \mu_2\rho_3\hat{x}\right)(\delta_1\hat{u} + \mu_1)\right]. \end{aligned} \quad (2.3)$$

We see that $b_i > 0, i = 1,2,3,4$, and if $\phi_2(p) > 0$ and $\phi_3(p) > 0$, then $b_1b_2 - b_3 > 0$ and $b_3(b_1b_2 - b_3) - b_1^2b_4 > 0$, so that $S_3 = (\hat{u},\hat{w},\hat{v},\hat{x},\hat{y})$ is LAS. If $\phi_2(p) < 0$ or $\phi_3(p) < 0$, then $b_1b_2 - b_3 < 0$ or $b_3(b_1b_2 - b_3) - b_1^2b_4 < 0$, respectively, so that S_3 is unstable when it exists. By [42], the system has a Hopf bifurcation at S_2 if and only if $\phi_3(p) = 0$, assuming $\mathcal{R}_0 > 1$ and $\mathcal{R}_1 \neq 1$, thereby $J(S_3)$ has a pair of pure imaginary eigenvalues $\lambda = \pm i\sqrt{b_3/b_1}$. □

Remark 2.2. Notice that if $(\rho_1/\mu_1 + \delta_1)\rho_2\hat{u} > \rho_1$, that is,

$$\rho_2\left(\frac{\rho_1}{\mu_1} + \delta_1\right)\left(1 - \frac{1}{\mathcal{R}_0} + \frac{1}{\mathcal{R}_0\mathcal{R}_1}\right) > \rho_1,$$

then $\phi_2(p) > 0$ and $\phi_3(p) > 0$, implying that $S_3 = (\hat{u},\hat{w},\hat{v},\hat{x},\hat{y})$ is LAS when it exists (i.e. $\mathcal{R}_0 > 1, \mathcal{R}_1 > 1$).

All these conditions are summarized in the Table 1.

Table 1: Summary of conditions for existence and LAS of equilibria S_1, S_2, S_3.

	$S_1(1,0,0,0,0)$	$S_2(\bar{u},\bar{w},\bar{v},0,0)$	$S_3(\hat{u},\hat{w},\hat{v},\hat{x},\hat{y})$
Existence	Always	$\mathcal{R}_0 > 1$	$\mathcal{R}_0 > 1, \mathcal{R}_1 > 1$
LAS (iff)	$\mathcal{R}_0 < 1$	$\mathcal{R}_0 > 1 > \mathcal{R}_1$, $\phi_1(p) > 0$	$\mathcal{R}_0 > 1, \mathcal{R}_1 > 1$, $\phi_2(p) > 0, \phi_3(p) > 0$
LAS (sufficient)		$\mathcal{R}_0 > 1 > \mathcal{R}_1$, $\delta_1 > \rho_2 + \left(\frac{\rho_1}{\rho_2} - 1\right)\mathcal{R}_0$	$\mathcal{R}_0 > 1, \mathcal{R}_1 > 1$, $\left(\frac{\rho_1}{\mu_1} + \delta_1\right)\rho_2\hat{u} > \rho_1$
Unstable	$\mathcal{R}_0 > 1$	$\mathcal{R}_0 > 1$ and ($\mathcal{R}_1 > 1$ or $\phi_1(p) < 0$)	$\mathcal{R}_0 > 1, \mathcal{R}_1 > 1$ and ($\phi_2(p) < 0$ or $\phi_3(p) < 0$)
Hopf bifurcation		$\mathcal{R}_0 > 1, \mathcal{R}_1 \neq 1$, $\phi_1(p) = 0$	$\mathcal{R}_0 > 1, \mathcal{R}_1 > 1$, $\phi_3(p) = 0$

Biological interpretation of epidemiological threshold parameters are given as follows: The basic reproduction number T

$$\mathcal{R}_0 = \frac{\rho_1}{\mu_1} + \rho_2 = \beta_1 T_M \frac{1}{d_I}\frac{\gamma}{d_V} + \beta_2 T_M \frac{1}{d_I}$$

combines two distinct infection pathways. The first term quantifies virus-to-cell transmission, where $\beta_1 T_M$ represents the infection rate when target cells (T_M) are abundant, $1/d_I$ is the average infectious period of an infected cell, and γ/d_V gives the total viral particles produced per cell during its lifespan. The second term characterizes cell-to-cell spread, where $\beta_2 T_M$ reflects the direct transmission rate between adjacent cells, with $1/d_I$ again representing the duration of infectiousness. Together, $\mathcal{R}_0$ estimates the expected secondary infections generated by a single infected cell through both free-virus diffusion and direct cellular transmission in a fully susceptible cell population.

The immune-response establishment threshold $\mathcal{R}_1 > 1$ implies

$$\frac{\delta_2 - \eta}{\mu_2}\delta_1 > \frac{\mathcal{R}_0^2}{\mathcal{R}_0 - 1},$$

that is

$$\frac{r_1 - \rho}{d_E} r_1 T_M > \frac{\mathcal{R}_0^2}{\mathcal{R}_0 - 1},$$

which biologically indicates that successful immune activation requires the following:

(i) sufficiently rapid immune cell proliferation (large δ_2 or r_1),

(ii) minimal immune exhaustion (small η or ρ),

(iii) long-lived immune effectors (small μ_2 or d_E),

(iv) abundant target cell availability (large δ_1 or $r_1 T_M$),

all of which must collectively overcome the viral replicative potential quantified by $\mathcal{R}_0^2/(\mathcal{R}_0 - 1)$, where this threshold increases with higher basic reproduction number $\mathcal{R}_0$ ($\mathcal{R}_0 > 2$), and decreases for $\mathcal{R}_0 < 2$.

2.3 Global stability of equilibria S_1 and S_2

In this section, we prove that S_1 is globally asymptotically stable (GAS) when $\mathcal{R}_0 < 1$, while S_2 is GAS if $\mathcal{R}_0 > 1, \mathcal{R}_1 < 1 - \epsilon$ and

$$\delta_1 > \max\left\{ \left(\frac{\rho_1}{\mu_1} + \rho_2 \mathcal{R}_0 s \right) \mathcal{R}_0, \rho_2 + \left(\frac{\rho_1}{\rho_2} - 1 \right) \mathcal{R}_0 \right\},$$

where $s := \max\{1/\mu_2, 1\}$, and ϵ is a small positive constant. We prove these results by constructing an appropriate Lyapunov functional, whose form is motivated by the Lyapunov function in [15, 22, 23]. We define the function $g(x) = x - 1 - \ln x$.

Theorem 2.4. *If $\mathcal{R}_0<1$, the infection-free equilibrium $S_1=(1,0,0,0,0)$ is GAS.*

Proof. Let $(u(t),w(t),v(t),x(t),y(t))$ be a solution of system (1.2) satisfying $u(t)>0$, and let

$$L_1(u,w,v,x,y)=g(u)+w+A_1v+A_2x+A_3y,$$

where $A_i, i=1,2,3$, are constants to be determined, then time derivative of L_1 along the solutions of (1.2) is

$$\begin{aligned}\frac{\mathrm{d}L_1}{\mathrm{d}t}&=\left(1-\frac{1}{u}\right)\frac{\mathrm{d}u}{\mathrm{d}t}+\frac{\mathrm{d}w}{\mathrm{d}t}+A_1\frac{\mathrm{d}v}{\mathrm{d}t}+A_2\frac{\mathrm{d}x}{\mathrm{d}t}+A_3\frac{\mathrm{d}y}{\mathrm{d}t}\\&=-\delta_1(1-u)^2+(\rho_1-A_1\mu_1)v+(\rho_2-1+A_1)w+(A_1\delta_2-\rho_3)xw-A_2(\mu_2x+\mu_3y).\end{aligned}$$

The constants $A_i>0, i=1,2,3,4$, are chosen to satisfy

$$\rho_1-A_1\mu_1<0,\quad \rho_2-1+A_1<0,\quad A_2\delta_2-\rho_3\le 0,$$

that is, $\mathcal{R}_0-\rho_2<A_1<1-\rho_2$ and $A_2\le\rho_3/\delta_2$. We take

$$A_1=\frac{\mathcal{R}_0+1-2\rho_2}{2},\quad A_2=\frac{\rho_3}{\delta_2},$$

then

$$\frac{\mathrm{d}L_1}{\mathrm{d}t}=-\delta_1(1-u)^2-\frac{\mu_1}{2}(1-\mathcal{R}_0)v-\frac{1}{2}(1-\mathcal{R}_0)w-\frac{\rho_3}{\delta_2}(\mu_2x+\mu_3y).$$

We see that if $\mathcal{R}_0<1$, then $\mathrm{d}L_1/\mathrm{d}t\le 0$, and

$$Q_1:=\left\{(u(t),w(t),v(t),x(t),y(t))\,\middle|\,\frac{\mathrm{d}L_1}{\mathrm{d}t}=0\right\}=\{(1,0,0,0,0)\}.$$

The largest invariant set in Q_1 is $\{S_1=(1,0,0,0,0)\}$, thus by the LaSalle invariance principle [21], all nonnegative solutions tend to S_1. Therefore, S_1 is globally attractive as $\mathcal{R}_0<1$. With the local asymptotic stability of S_1, we get that S_1 is GAS. □

Lemma 2.2. *If $\mathcal{R}_0>1$ and $\delta_1>\rho_1/\mu_1+\rho_2\mathcal{R}_0s$, then for any solution $(u(t),w(t),v(t),x(t),y(t))\in\mathbb{X}, (u(t)>0)$, of system (1.2), with initial condition $(u(0),w(0),v(0),x(0),y(0))\in\mathbb{X}, (u(0)>0)$, we have*

$$\liminf_{t\to+\infty}u(t)\ge 1-\frac{\rho_1/\mu_1+\rho_2\mathcal{R}_0s}{\delta_1},$$

where $s:=\max\{1/\mu_2,1\}$.

Proof. For any solution $(u(t),w(t),v(t),x(t),y(t))\in\mathbb{X}, (u(t)>0)$, of system (1.2), with initial condition $(u(0),w(0),v(0),x(0),y(0))\in\mathbb{X}, (u(0)>0)$, from the proof of Theorem 2.1, we see that

$$\limsup_{t\to+\infty}v(t)\le\frac{1}{\mu_1},\quad \limsup_{t\to+\infty}w(t)\le\frac{\rho_3}{\delta_2-\eta}\zeta=\mathcal{R}_0s.$$

Hence, for $\epsilon>0$ sufficiently small, there is a $T_1>0$ such that if $t>T_1$, then

$$v(t)<\frac{1}{\mu_1}+\epsilon,\quad w(t)<\mathcal{R}_0 s+\epsilon,$$

so that from the Eq. (1.2a),

$$\frac{\mathrm{d}u}{\mathrm{d}t}\geq\delta_1 u(1-u)-\left(\frac{\rho_1}{\mu_1}+\rho_1\epsilon+\rho_2(\mathcal{R}_0 s+\epsilon)\right)u.$$

By a standard comparison argument, it follows that

$$\liminf_{t\to+\infty}u(t)\geq 1-\frac{\rho_1/\mu_1+\rho_1\epsilon+\rho_2(\mathcal{R}_0 s+\epsilon)}{\delta_1}.$$

Since $\epsilon>0$ is arbitrarily sufficiently small, we therefore obtain

$$\liminf_{t\to+\infty}u(t)\geq 1-\frac{\rho_1/\mu_1+\rho_2\mathcal{R}_0 s}{\delta_1}.$$

This completes the proof. □

Theorem 2.5. *If $\mathcal{R}_0>1,\mathcal{R}_1<1-\epsilon$ and*

$$\delta_1>\max\left\{\left(\frac{\rho_1}{\mu_1}+\rho_2\mathcal{R}_0 s\right)\mathcal{R}_0,\rho_2+\left(\frac{\rho_1}{\rho_2}-1\right)\mathcal{R}_0\right\},$$

the uncontrolled-infection equilibrium $S_2=(\bar{u},\bar{w},\bar{v},0,0)$ is GAS, where $s:=\max\{1/\mu_2,1\}$, and ϵ is a small constant.

Proof. Let $(u(t),w(t),v(t),x(t),y(t))$ be a solution of system (1.2) satisfying $u(t)>0$, $w(t)>0,v(t)>0$, and let

$$L_2(u,w,v,x,y)=\bar{u}g\left(\frac{u}{\bar{u}}\bar{v}\right)+\bar{w}g\left(\frac{w}{\bar{w}}\right)+\frac{\rho_1\bar{u}}{\mu_1}\bar{v}g\left(\frac{v}{\bar{v}}\right)+\frac{\rho_3\bar{w}}{\mu_2}x+\frac{\rho_3\epsilon}{\eta}y,$$

where ϵ is a small constant. The time derivative of L_2 along the solutions of (1.2) is given by

$$\begin{aligned}\frac{\mathrm{d}L_2}{\mathrm{d}t}&=\left(1-\frac{\bar{u}}{u}\right)\frac{\mathrm{d}u}{\mathrm{d}t}+\left(1-\frac{\bar{w}}{w}\right)\frac{\mathrm{d}w}{\mathrm{d}t}+\frac{\rho_1\bar{u}}{\mu_1}\left(1-\frac{\bar{v}}{v}\right)\frac{\mathrm{d}v}{\mathrm{d}t}+A_3\frac{\mathrm{d}x}{\mathrm{d}t}+A_4\frac{\mathrm{d}y}{\mathrm{d}t}\\&=\left(1-\frac{\bar{u}}{u}\right)[\delta_1 u(1-u)-(\rho_1 v+\rho_2 w)u]+\left(1-\frac{\bar{w}}{w}\right)[(\rho_1 v+\rho_2 w)u-w-\rho_3 xw]\\&\quad+\frac{\rho_1\bar{u}}{\mu_1}\left(1-\frac{\bar{v}}{v}\right)[w-\mu_1 v]+\frac{\rho_3\bar{w}}{\mu_2}[(\delta_2-\eta)w-\mu_2]x+\frac{\rho_3\epsilon}{\eta}(\eta xw-\mu_3 y).\end{aligned}$$

Applying

$$\delta_1\bar{u}(1-\bar{u})=(\rho_1\bar{v}+\rho_2\bar{w})\bar{u},\quad (\rho_1\bar{v}+\rho_2\bar{w})\bar{u}=\bar{w},\quad \bar{w}=\mu_1\bar{v},$$

it follows that

$$\begin{aligned}\frac{\mathrm{d}L_2}{\mathrm{d}t}=&\left(1-\frac{\bar{u}}{u}\right)[\delta_1u(1-u)-\delta_1\bar{u}(1-\bar{u})]+(\rho_1\bar{v}+\rho_2\bar{w})\left(\bar{u}-\frac{\bar{u}^2}{u}\right)+(\rho_1v+\rho_2w)(\bar{u}-u)\\&+[(\rho_1v+\rho_2w)u-w]-\left(\rho_1v\frac{\bar{w}}{w}+\rho_2\bar{w}\right)u+(\rho_1\bar{v}+\rho_2\bar{w})\bar{u}\\&+\frac{\rho_1\bar{u}}{\mu_1}w-\rho_1\bar{u}v-\frac{\rho_1\bar{u}}{\mu_1}\frac{\bar{v}}{v}w+\rho_1\bar{v}\bar{u}-\rho_3xw+\rho_3x\bar{w}\\&+\frac{\rho_3\bar{w}}{\mu_2}[(\delta_2-\eta)xw-\mu_2x]+\frac{\rho_3\epsilon}{\eta}(\eta xw-\mu_3y)\\=&\delta_1\frac{(u-\bar{u})^2}{u}[1-(u+\bar{u})]+\rho_1\bar{v}\bar{u}\left(3-\frac{\bar{u}}{u}-\frac{w\bar{v}}{\bar{w}v}-\frac{u\bar{w}v}{\bar{u}w\bar{v}}\right)+\rho_2\bar{w}\bar{u}\left(2-\frac{\bar{u}}{u}-\frac{u}{\bar{u}}\right)\\&+\rho_3(\mathcal{R}_1-1+\epsilon)xw-\frac{\rho_3\mu_3\epsilon}{\eta}y.\end{aligned}$$

From Lemma 2.2, if $\mathcal{R}_0>1$ and $\delta_1>\rho_1/\mu_1+\rho_2\mathcal{R}_0s$, there is a $T>0$ such that for $t>T$,

$$u(t)\geq 1-\frac{\rho_1/\mu_1+\rho_2\mathcal{R}_0s}{\delta_1}.$$

If $\delta_1>(\rho_1/\mu_1+\rho_2\mathcal{R}_0s)\mathcal{R}_0$, it follows that, for $t>T$,

$$u>1-\frac{1}{\mathcal{R}_0}=1-\bar{u},$$

so that

$$\delta_1\frac{(u-\bar{u})^2}{u}[1-(u+\bar{u})]\leq 0$$

with equality if and only if $u(t)=\bar{u}$. Due to the arithmetic-geometric mean inequality,

$$3-\frac{\bar{u}}{u}-\frac{w\bar{v}}{\bar{w}v}-\frac{u\bar{w}v}{\bar{u}w\bar{v}}\leq 0,\quad 2-\frac{\bar{u}}{u}-\frac{u}{\bar{u}}\leq 0.$$

We see that if $\mathcal{R}_1<1-\epsilon$, then $\mathrm{d}L_2/\mathrm{d}t\leq 0$. Let

$$Q_2=\left\{(u,w,v,x,y)\,\middle|\,\frac{\mathrm{d}L_2}{\mathrm{d}t}=0\right\},$$

then

$$Q_2=\left\{(u,w,v,x,y)\,\middle|\,u=\bar{u},\frac{w}{\bar{w}}=\frac{v}{\bar{v}},x=0,y=0\right\}=\{(\bar{u},\bar{w},\bar{v},0,0)\}.$$

Here, $w/\bar{w}=v/\bar{v}$ implies that

$$\frac{\mathrm{d}v}{\mathrm{d}t}=\left(\frac{\bar{w}}{\bar{v}}-\mu_1\right)v=0,$$

thus $v=\bar{v}$, and furthermore $w=\bar{w}$. The largest invariant set in Q_2 is $\{S_2=(\bar{u},\bar{w},\bar{v},0,0)\}$, thus by the LaSalle invariance principle [21], all nonnegative solutions tend to S_2. Therefore, S_2 is globally attractive under $\mathcal{R}_0>1, \mathcal{R}_1<1-\epsilon$ and $\delta_1>(\rho_1/\mu_1+\rho_2\mathcal{R}_0 s)\mathcal{R}_0$, and furthermore it is GAS, if $\delta_1>\rho_2+(\rho_1/\rho_2-1)\mathcal{R}_0$. □

Remark 2.3. The stability conditions

$$\delta_1>\rho_2+\left(\frac{\rho_1}{\rho_2}-1\right)\mathcal{R}_0,\quad \delta_1>\left(\frac{\rho_1}{\mu_1}+\rho_2\mathcal{R}_0 s\right)\mathcal{R}_0,$$

where $s:=\max\{1/\mu_2,1\}$, indicate that viral persistence (stable S_2) under weak immunity ($\mathcal{R}_1<1$) requires high CD4$^+$ T cell supply (large δ_1) in contrast to the infection rates (ρ_1 and ρ_2) to sustain infection.

3 Numerical simulation

3.1 Parameter estimation and numerical methods

We derived the apoptosis/degradation rates in the model from empirical half-life data. For free HIV virions, half-life $t_{1/2}=0.1$ (range: 30min$-$0.24 days [25]), yielding $d_V=\ln(2)/t_{1/2}=\ln(2)/0.1=6.9315$/day. For virus-producing virus-producing CD4$^+$ T cells, $t_{1/2}=0.7$ days [3], giving $d_I=\ln(2)/0.7=0.9902$/day. For the early-stage exhausted CD8$^+$ T cells, half-life $t_{1/2}=10$ days (range: 1–2 weeks), resulting in $d_E=\ln(2)/10=0.0693$/day. Terminally exhausted CD8$^+$ T cells have a reduced half-life $t_{1/2}=5$ days, due to PD-1/Blimp-1-driven apoptosis [26], leading to $d_{E^*}=\ln(2)/5=0.1386$/day. According to [6], we set $r_1=0.1$/day, $T_M=1000$, $\gamma=200$, $E_M=1000$. The other parameters that related to infection (β_1, β_2) and CD8$^+$ T cell response (r_2, ρ, α) are fitted to 5-year longitudinal data from a slow CD4 decline patient (Patient D in [33]).

To identify the optimal parameter set $\vec{p}=\{\beta_1,\beta_2,r_2,\rho,\alpha\}$, we minimized the sum of squared normalized errors (SSNE) between cohort data and model simulations, defined as

$$\min_{\vec{p}} SE(\vec{p})=\sum_{j=1}^{m}\left(\frac{\hat{X}(t_j)-X(t_j,\vec{p})}{\max\left(\hat{X}(t_j)\right)}\right)^2,$$

where $\hat{X}(t_j)$ denotes the observed cohort data at time t_j, and represents the simulated output with parameters $\vec{p}$. Initial conditions are derived from cohort measurements: viral load copies/mL, and cell counts $T(0)=115.2054, I(0)=5.7603, E(0)=84.8352, E^*(0)=84.8352$cells/$\mu$L blood.

We applied the particle swarm optimization (PSO) [16] combined with Latin hypercube sampling (LHS) [24] to optimize the objective function and find the best fit parameter values. The agreement between cohort data and model simulations is presented in Fig.1. The goodness of fit is SSNE$=0.43$ and the resulting parameter values

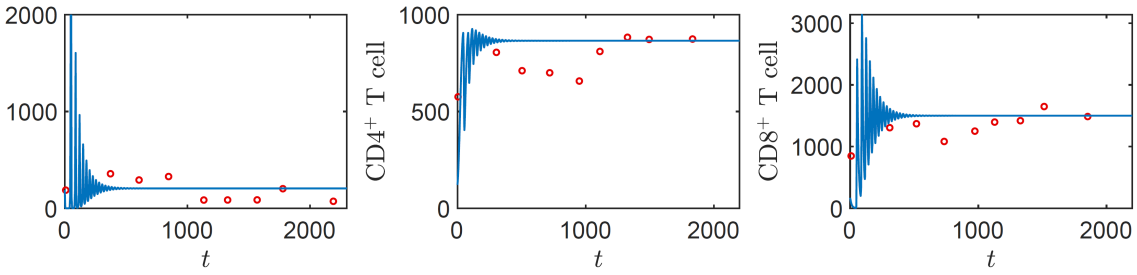

Figure 1: The dynamics of CD4$^+$ T and CD8$^+$ T-cell and viral load. CD4$^+$ and CD8$^+$ T-cell (per ml blood) and viral load (log copies/ml) dynamics with HIV-infected clinical data (red) and simulation (blue) by the model (1.1). The time scale is in day.

are $\beta_1 = 5.1079\times10^{-5}, \beta_2 = 5.102\times10^{-4}, r_2 = 0.0327, \rho = 0.023$ and $\alpha = 0.001$. The corresponding non-dimensionalized parameter values are $\delta_1 = 0.1010, \rho_1 = 10.4190, \rho_2 = 0.5152$, $\rho_3 = 1.0099, \delta_2 = 33.0236, \eta = 23.2276, \mu_1 = 7.0001, \mu_2 = 0.0700$ and $\mu_3 = 0.1400$.

We note a divergence in long-term dynamics: In the early-phase, the model predicts initial oscillations (likely reflecting immune-viral feedback loops) that are not observed in the cohort data, possibly due to limited sampling frequency in clinical measurements; in the late-phase, the longitudinal data exhibits sustained low-amplitude fluctuations (consistent with persistent immune activity), whereas our simulations converge to steady states. This discrepancy may arise from our model simplifications (e.g. constant parameter values vs. biological variability). Incorporating noise-driven dynamics or time-dependent parameters could bridge this gap (e.g. via stochastic differential equations or periodic forcing), which we will not consider in this paper. We now turn to examining the bifurcation dynamics of the system and the impacts of CD8$^+$ T cell exhaustion on these dynamics.

All model simulations are performed in MATLAB R2019a using the solvers `ode45` and `ode23`, with relative and absolute tolerance equal to 1e-6. Bifurcation thresholds are determined by computing via Maple 2021. The Hopf bifurcation points are detected by eigenvalue monitoring ($\mathrm{Re}(\lambda) = 0, \mathrm{Im}(\lambda) \neq 0$) using Maple 2021.

3.2 Bifurcation diagram

We analyze the system with high exhaustion rate ($\eta = 27$), using ρ_1 as the bifurcation parameter that is related to all the thresholds of model dynamics, that is, $\mathcal{R}_0, \mathcal{R}_1, \phi_1, \phi_2$ and ϕ_3 (see Eqs. (2.1)-(2.3)). Fig. 2(a) shows these threshold functions versus ρ_1:

(i) The basic reproduction number $\mathcal{R}_0(\rho_1)$ increases linearly, crossing 1 at $\rho_1^{c_0} = 3.3936$. The infection-free state $S_1 = (1,0,0,0,0)$ is LAS for $\rho_1 < \rho_1^{c_0}$ (i.e. $\mathcal{R}_0(\rho_1) < 1$), but lose stability when $\rho_1 > \rho_1^{c_0}$ (i.e. $\mathcal{R}_0(\rho_1) > 1$). A transcritical bifurcation occurs at S_1 as ρ_1 passes $\rho_1 = \rho_1^{c_0}$, and the uncontrolled-infection state $S_2 = (\bar{u}, \bar{w}, \bar{v}, 0, 0)$ appears for $\rho_1 > \rho_1^{c_0}$.

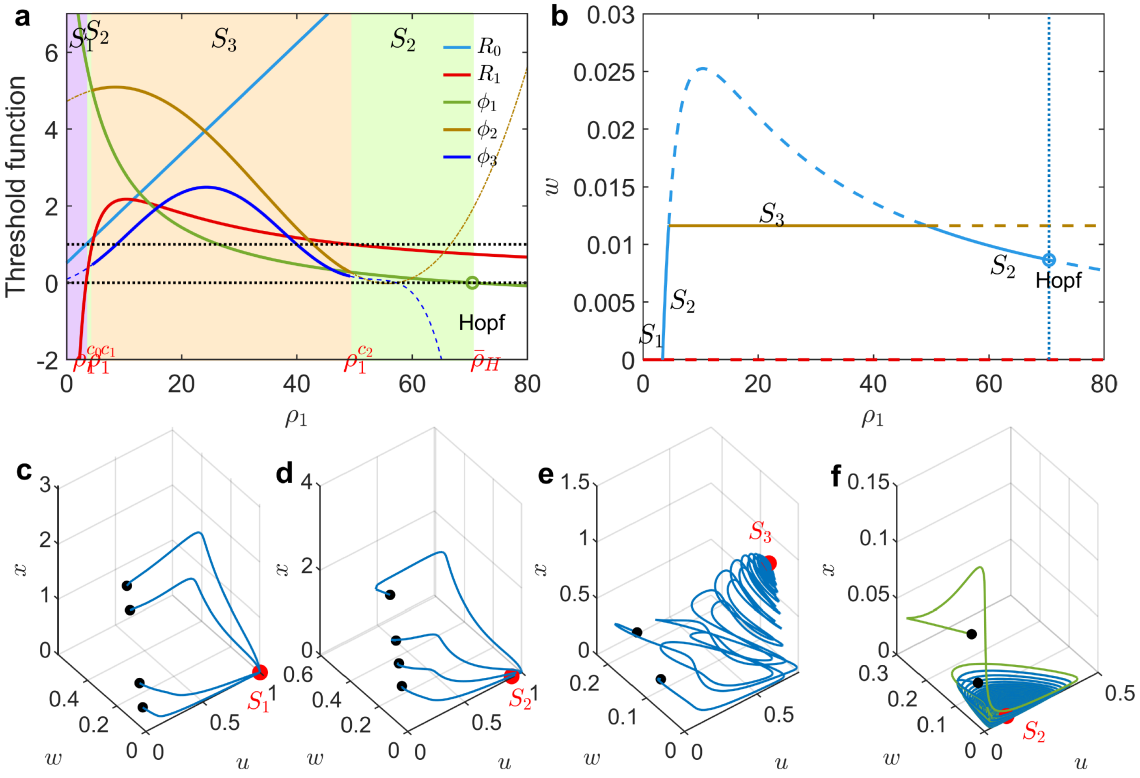

Figure 2: Bifurcation diagram and phase space portrait under high exhaustion rate $\eta=27$. (a) The curves of threshold functions $\mathcal{R}_0(\rho_1),\mathcal{R}_1(\rho_1),\phi_1(\rho_1),\phi_2(\rho_1),\phi_3(\rho_1)$. (b) The bifurcation of equilibrium level of infected cells w with respect to ρ_1. The solid curves indicate LAS equilibrium, while dashed curves denote corresponding unstable equilibria. (c)-(f) Phase space portraits. The black dots denote the initial value point, while the red dots indicate equilibria. (c) $S_1=(1,0,0,0,0)$ is LAS with $\rho_1=1\in(0,\rho_1^{c_0})$. (d) $S_2=(\bar{u},\bar{w},\bar{v},0,0)$ is LAS with $\rho_1=4\in(\rho_1^{c_0},\rho_1^{c_1})$. (e) $S_3=(\hat{u},\hat{w},\hat{v},\hat{x},\hat{y})$ is LAS with $\rho_1=20\in(\rho_1^{c_1},\rho_1^{c_2})$. (f) $S_2=(\bar{u},\bar{w},\bar{v},0,0)$ is LAS with $\rho_1=60\in(\rho_1^{c_2},\bar{\rho}_H)$.

(ii) The immune response threshold $\mathcal{R}_1(\rho_1)$ is a concave function, intersecting 1 at two points $\rho_1^{c_1}=4.4642$ and $\rho_1^{c_2}=49.1620$. The stability threshold $\phi_1(\rho_1)$ for $S_2=(\bar{u},\bar{w},\bar{v},0,0)$ is a convex function within the range $\rho_1\in[0,100]$, with a zero point at $\rho_1=\bar{\rho}_H=70.4075$. Note that $\bar{\rho}_H>\rho_1^{c_2}$, so that the uncontrolled-infection state S_2 is LAS, when $\rho_1^{c_0}<\rho_1<\rho_1^{c_1}$ (i.e. $\mathcal{R}_0(\rho_1)>1,\mathcal{R}_1(\rho_1)<1,\phi_1(\rho_1)>0$), while it becomes unstable for $\rho_1^{c_1}<\rho_1<\rho_1^{c_2}$ (i.e. $\mathcal{R}_1(\rho_1)>1$). We see that the system also experience a transcritical bifurcation at S_2 as ρ_1 crosses $\rho_1=\rho_1^{c_1}$, and the immune-controlled state $S_3=(\hat{u},\hat{w},\hat{v},\hat{x},\hat{y})$ appears for $\rho_1>\rho_1^{c_1}$ (i.e. $\mathcal{R}_1(\rho_1)>1$).

(iii) The stability thresholds $\phi_2(\rho_1)$ and $\phi_3(\rho_1)$ of S_3 are all positive for $\rho_1^{c_1}<\rho_1<\rho_1^{c_2}$ (where $\mathcal{R}_1(\rho_1)>1$), thereby S_3 is LAS.

(iv) As ρ_1 passes $\rho_1=\rho_1^{c_2}$, a transcritical bifurcation occurs and the stability of S_2 and S_3 exchanges. The uncontrolled-infection state S_2 is LAS for $\rho_1^{c_2}<\rho_1<\bar{\rho}_H$.

Fig. 2(b) shows the corresponding bifurcation diagram of infected cells w. The local stability of $S_i, i=1,2,3$, are shown in 3D-phase portraits of (u,w,x) in Fig. 2(c-f), for ρ_1 taken in ranges $(0,\rho_1^{c_0}),(\rho_1^{c_0},\rho_1^{c_1}),(\rho_1^{c_1},\rho_1^{c_2})$ and $(\rho_1^{c_2},\bar{\rho}_H)$, respectively.

At the critical value $\rho_1=\bar{\rho}_H=70.4075$ (approximately), where $\phi_1(\bar{\rho}_H)=0$, the Jacobian matrix $J(S_2)$ of the linearized system at $S_2=(\bar{u},\bar{w},\bar{v},0,0)=(0.0946,0.0086,0.0012,0,0)$ possesses a pair of purely imaginary eigenvalues, $\lambda=\pm i\omega$, where $\omega=0.2836$, so that as ρ_1 crosses $\rho_1=\bar{\rho}_H$, a Hopf bifurcation occurs at S_2, and periodic solutions bifurcates from S_2 (see Fig. 3). For $\rho_1=65<\bar{\rho}_H$, the equilibrium $S_2=(\bar{u},\bar{w},\bar{v},0,0)$ remains stable, which is shown in the first column of Fig. 3, demonstrating phase portraits in (u,w) and (u,w,x) spaces, and time evolution of $x(t)$. As ρ_1 passes $\bar{\rho}_H$ and take $\rho_1=71>\bar{\rho}_H$, a stable limit cycle emerges, where only the susceptible cells $(u(t))$, infected cells $(w(t))$ and viral populations $(v(t))$ exhibit sustained oscillations, whereas the immune cells (CD8$^+$ T cells, $x(t)$ and $y(t)$) vanish (see the second column of Fig. 3). This periodic behavior persists for larger ρ_1 values, for example, for $\rho_1=75>\bar{\rho}_H$, the system also has stable periodic solutions (see the third column of Fig. 3).

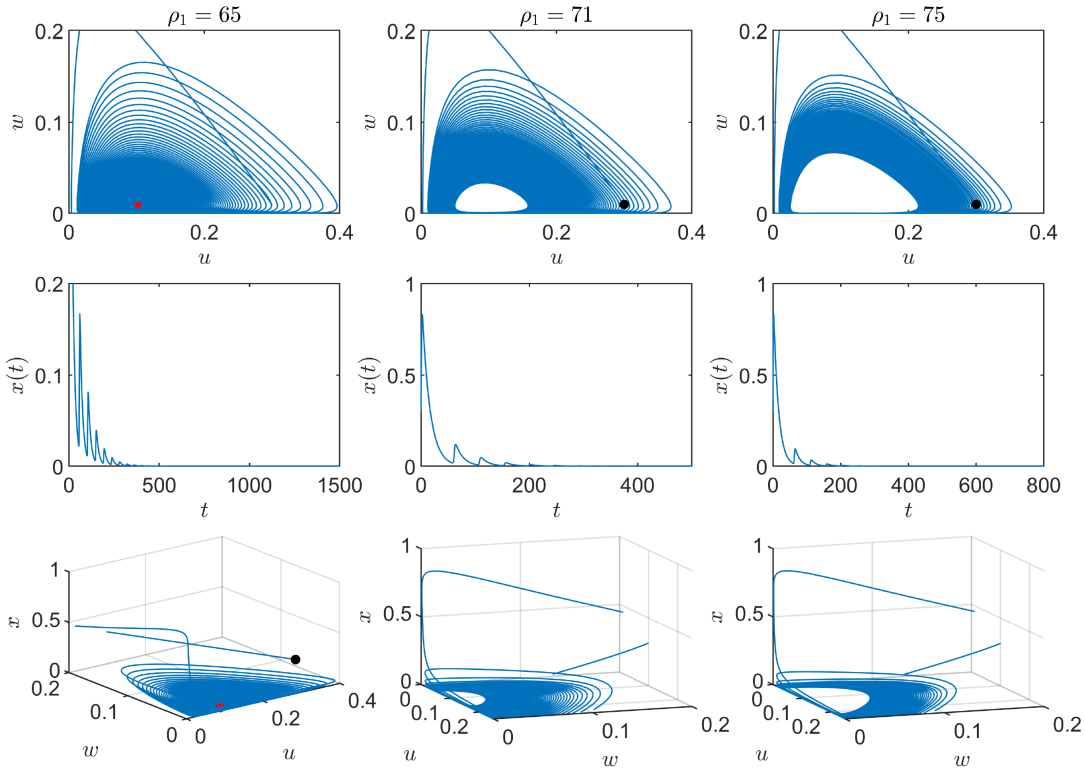

Figure 3: Hopf bifurcation at S_2 as ρ_1 passes $\rho_1=\bar{\rho}_H$ under high exhaustion rate $\eta=27$. The three subplots in the first column show stability of $S_2=(\bar{u},\bar{w},\bar{v},0,0)$ for $\rho_1=65<\rho_H$. The green dot in the first subplot indicates S_2. The three subplots in the second column demonstrate the limit cycle bifurcated from S_2 for $\rho_1=71>\bar{\rho}_H$. The three subplots in the third column present the existence of stable limit cycle for $\rho_1=75>\bar{\rho}_H$. The initial value points are denoted by black dots.

We examine the system with the fitted exhaustion rate ($\eta=23.2276$), where the threshold functions $\mathcal{R}_0(\rho_1),\mathcal{R}_1(\rho_1),\phi_1(\rho_1)$, $\phi_2(\rho_1)$ and $\phi_3(\rho_1)$ (see Fig. 4(a)). exhibit similar profiles to the high-exhaustion case for $\rho_1\in[0,80]$ but with shifted bifurcation points. Wile the basic production number $\mathcal{R}_0(\rho_1)$ still crosses 1 at $\rho_1^{c_0}=3.3936$, the immune response threshold $\mathcal{R}_1(\rho_1)$ passes 1 at two points $\rho_1^{c_1}=3.9745$ and $\rho_1^{c_2}=87.7536$. The stability thresholds $\phi_1(\rho_1)$-$\phi_3(\rho_1)$ have zeros at $\rho_1^{c_3}=70.4075,\rho_1^{c_4}=84.0218$, and $\rho_1=\bar{\rho}_H=78.2991$, respectively. Noticing that $\rho_1^{c_0}<\rho_1^{c_1}<\rho_1^{c_3}<\bar{\rho}_H<\rho_1^{c_4}<\rho_1^{c_2}$, we have the bifurcation as shown in Fig. 4(b). The infection-free equilibrium $S_1=(1,0,0,0,0)$ is LAS for $\rho_1<\rho_1^{c_0}$ (i.e. $\mathcal{R}_0(\rho_1)<1$), and transcritical bifurcation occurs at S_1 as ρ_1 passes $\rho_1=\rho_1^{c_0}$, and the uncontrolled-infection state $S_2=(\bar{u},\bar{w},\bar{v},0,0)$ appears, which is LAS for $\rho_1^{c_0}<\rho_1<\rho_1^{c_1}$ (i.e. $\mathcal{R}_0(\rho_1)>1,\mathcal{R}_1(\rho_1)<1$ and $\phi_1(\rho_1)>0$). When ρ_1 crosses $\rho_1=\rho_1^{c_1}$, the system also experiences a transcritical bifurcation at S_2, and the immune-controlled state $S_3=(\hat{u},\hat{w},\hat{v},\hat{x},\hat{y})$ appears, which is LAS for $\rho_1^{c_1}<\rho_1<\bar{\rho}_H$. The local stability of $S_i,i=1,2,3$, are visualized

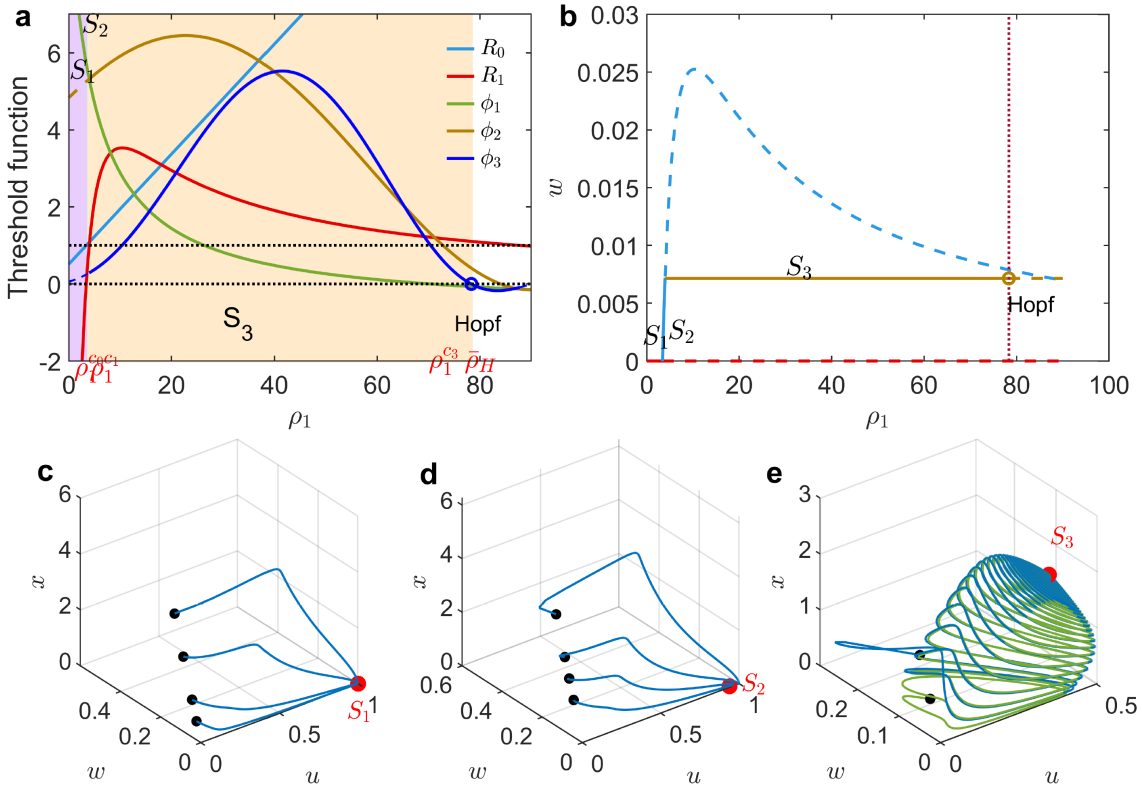

Figure 4: Bifurcation diagram and phase space portrait under exhaustion rate $\eta=23.2276$. (a) The curves of threshold functions $\mathcal{R}_0(\rho_1),\mathcal{R}_1(\rho_1),\phi_1(\rho_1),\phi_2(\rho_1),\phi_3(\rho_1)$. (b) The bifurcation of equilibrium level of infected cells w with respect to ρ_1. The solid curves indicate stable equilibrium, while dashed curves denote corresponding unstable equilibria. (c)-(f) Phase space portraits. The black dots denote the initial value point, while the red dots indicate the equilibria. (c) $S_1=(1,0,0,0,0)$ is LAS with $\rho_1=1\in(0,\rho_1^{c_0})$. (d) $S_2=(\bar{u},\bar{w},\bar{v},0,0)$ is LAS with $\rho_1=3.8\in(\rho_1^{c_0},\rho_1^{c_1})$. (e) $S_3=(\hat{u},\hat{w},\hat{v},\hat{x},\hat{y})$ is LAS with $\rho_1=60\in(\rho_1^{c_1},\bar{\rho}_H)$.

in 3D phase portraits of (u,w,x) in Figs. 4(c-e), for ρ_1 taken in ranges $(0,\rho_1^{c_0})$, $(\rho_1^{c_0},\rho_1^{c_1})$ and $(\rho_1^{c_1},\bar{\rho}_H)$, respectively.

At the critical value $\rho_1=\bar{\rho}_H=78.2991$, $\phi_3(\bar{\rho}_H)=0$, the Jacobian matrix $J(S_3)$ of the linearized system at $S_3=(\hat{u},\hat{w},\hat{v},\hat{x},\hat{y})=(0.1722,0.0071,0.0010,1.0046,1.1911)$ exhibits a pair of pure imaginary eigenvalues, $\lambda=\pm i\omega$, where $\omega=0.433091$, indicating a Hopf bifurcation as ρ_1 crosses $\rho_1=\bar{\rho}_H$. This bifurcation gives rise to periodic solutions, which are illustrated in Fig. 5. For $\rho_1=70,75<\bar{\rho}_H$, the equilibrium $S_2=(\hat{u},\hat{w},\hat{v},\hat{x},\hat{y})$ remains stable (see first and second columns of Fig. 5). As ρ_1 passes $\bar{\rho}_H$ and take $\rho_1=80>\bar{\rho}_H$, the system has stable limit cycle (see third column of Fig. 5). Notice that in this situation, all the populations $(u(t),w(t),v(t),x(t),y(t))$ persist with sustained oscillations.

Quantitative comparison reveals that $CD8^+$ T cell exhaustion also alters system attractors: Under low-exhaustion rate, $S_3=(\hat{u},\hat{w},\hat{v},\hat{x},\hat{y})$ is stable across a wide parameter range $\rho_1\in(\rho_1^{c_1},\bar{\rho}_H)=(3.9745,70.4075)$, whereas for high-exhaustion rate, S_3 is sta-

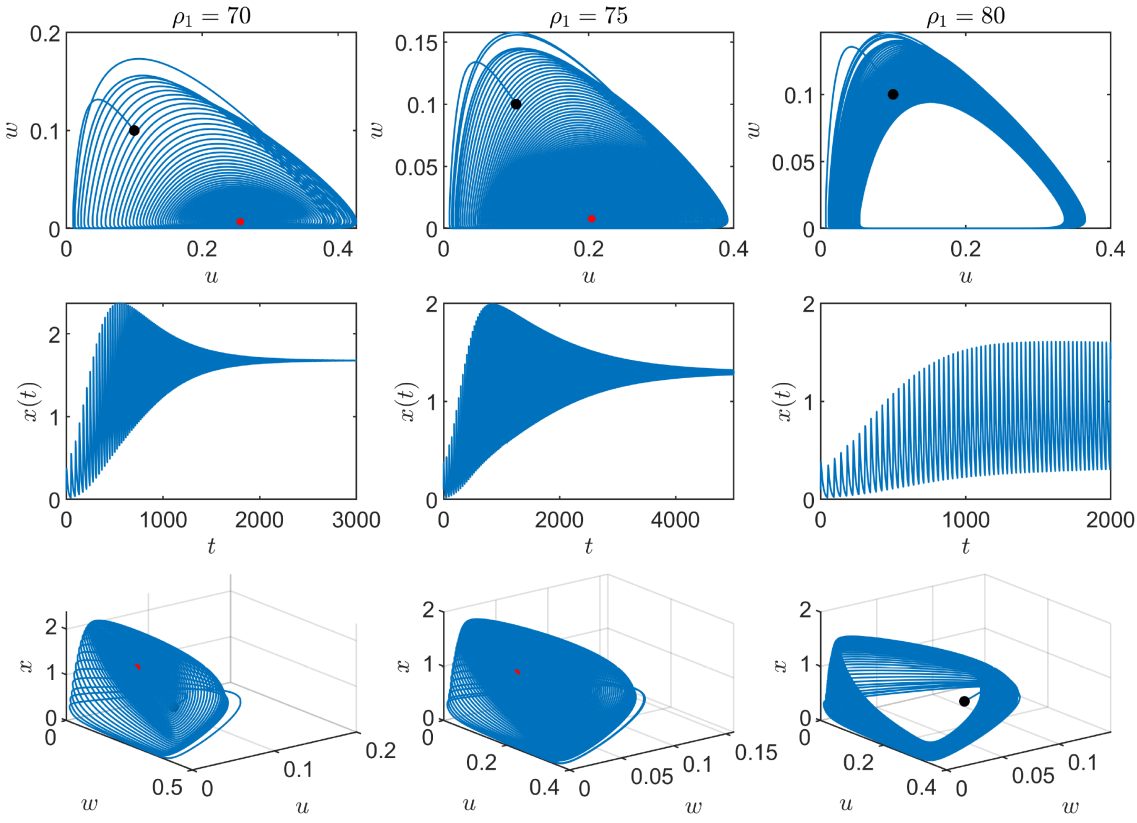

Figure 5: Hopf bifurcation at S_3 as ρ_1 passes $\rho_1=\bar{\rho}_H$ under exhaustion rate $\eta=23.2276$. The three subplots in the first column show stability of $S_3=(\hat{u},\hat{w},\hat{v},\hat{x},\hat{y})$ for $\rho_1=\bar{7}0$, with phase portrait in (u,w)-plane, time evolution of $x(t)$, and phase portrait in (u,w,x)-space, respectively. The green dot indicates S_3. The three subplots in the third column demonstrate the limit cycle bifurcated from S_3 for $\rho_1=80$. The initial value points are denoted by black dots.

ble only in a much narrower infection rate range $(\rho_1^{c_1},\rho_1^{c_2})=(4.4642,49.1620)$ with $S_2=(\bar{u},\bar{w},\bar{v},0,0)$ dominating other regimes ($\rho_1\in(\rho_1^{c_0},\rho_1^{c_1})=(3.3936,4.4642)$ and $\rho_1\in(\rho_1^{c_2},\bar{\rho}_H)=(49.1620,70.4075)$). This exhaustion-dependent bifurcation structure fundamentally modulates infection outcomes, as we explore below.

3.3 The effects of CD8$^+$ T cell exhaustion

To examine how CD8$^+$ T cell exhaustion influences viral infection dynamics, we selected η and ρ_1 as bifurcation parameters while keeping other parameters fixed (as in previous analyses). Fig. 6 presents the bifurcation diagram across $(\rho_1,\eta)\in[0,100]\times[0,32]$, revealing four distinct dynamical regimes:

(1) In region I ($\rho_1<3.3936$), the infection-free equilibrium $S_1=(1,0,0,0,0)$ is LAS, indicating viral clearance when infection rates are sufficiently low.

(2) Region II shows LAS for the uncontrolled-infection state $S_2=(\bar{u},\bar{w},\bar{v},0,0)$, demonstrating how high exhaustion rates (η) prevent immune control of infection.

(3) Region III exhibits LAS for the immune-controlled state $S_3=(\hat{u},\hat{w},\hat{v},\hat{x},\hat{y})$, occurring when either exhaustion or infection rates remain low.

(4) Regions IV$_1$, IV$_2$ and IV$_3$ display more complex dynamics: in IV$_1$, only unstable S_2 exists with periodic solutions bifurcated from S_1, while IV$_2$ and IV$_3$ contain both unstable S_2 and S_3 equilibria with periodic solutions bifurcating from S_3.

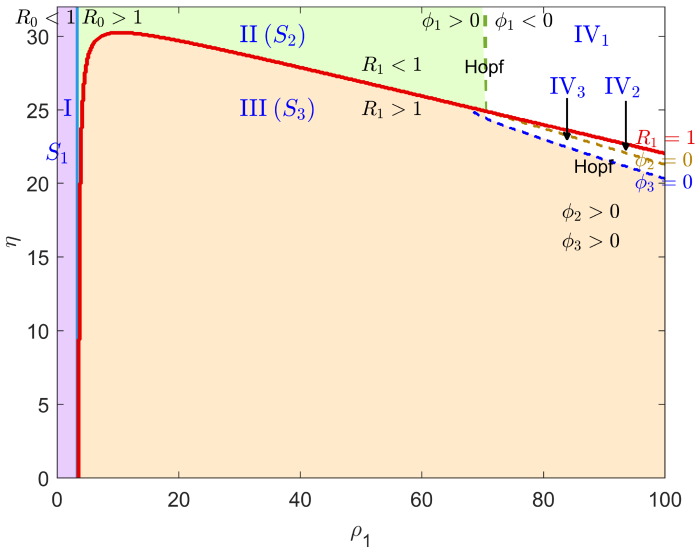

Figure 6: Bifurcation diagram with respect to ρ_1 and η. The parameter region $[0,100]\times[0,32]$ is separated into six regions (I, II, III, IV$_1$, IV$_2$, IV$_3$) by the threshold curves $\mathcal{R}_0(\rho_1,\eta)=1,\mathcal{R}_1(\rho_1,\eta)=1$, and $\phi_i(\rho_1,\eta)=0,i=1,2,3$. In region I, $\mathcal{R}_0<1$, where S_1 is LAS. In region II, $\mathcal{R}_0>1,\mathcal{R}_1<1$ and $\phi_1>0$, so that S_2 is LAS. In region III, $\mathcal{R}_0>1,\mathcal{R}_1>1,\phi_2>0$ and $\phi_3>0$, where S_3 is LAS. In regions IV$_1$ ($\mathcal{R}_0>1,\mathcal{R}_1<1,\phi_1<0$), IV$_2$ ($\mathcal{R}_0>1,\mathcal{R}_1>1$, $\phi_i<0,i=1,2,3$) and IV$_3$ ($\mathcal{R}_0>1,\mathcal{R}_1>1,\phi_i<0,i=1,3,\phi_2>0$), periodic solutions bifurcate from S_2 or S_3.

Fig. 7 illustrates the equilibrium distributions of infected cells (w), CD8$^+$ T cells (x), and exhausted CD8$^+$ T cells (y) across the (ρ_1,η) parameter space. Three distinct dynamical regimes emerge:

(1) In regions II and IV where T cell exhaustion rates are high, infected cell populations reach elevated equilibrium levels (with oscillatory dynamics in region IV; Figs. 7(a,d)), while both functional (x) and exhausted (y) CD8$^+$ T cell populations are depleted (Figs. 7(b-c)).

(2) When exhaustion rates are sufficiently low, CD8$^+$ T cells persist (see Fig. 7(e)), enabling effective viral control with minimal infected cell populations.

(3) At intermediate exhaustion rates coupled with low infection rates, the system exhibits high levels of exhausted CD8$^+$ T cells (see Fig. 7(f)) accompanied by progressive expansion of infected cells.

The bifurcation diagram (Fig. 6) and equilibrium distributions (Fig. 7) reveal periodic solutions in regions IV$_1$-IV$_3$ of the $(\rho_1,\eta)\in$ parameter space. To characterize these oscillations, we examine a representative case at $\rho_1=80$ (see Fig. 8), where the system undergoes sequential transitions as η increases:

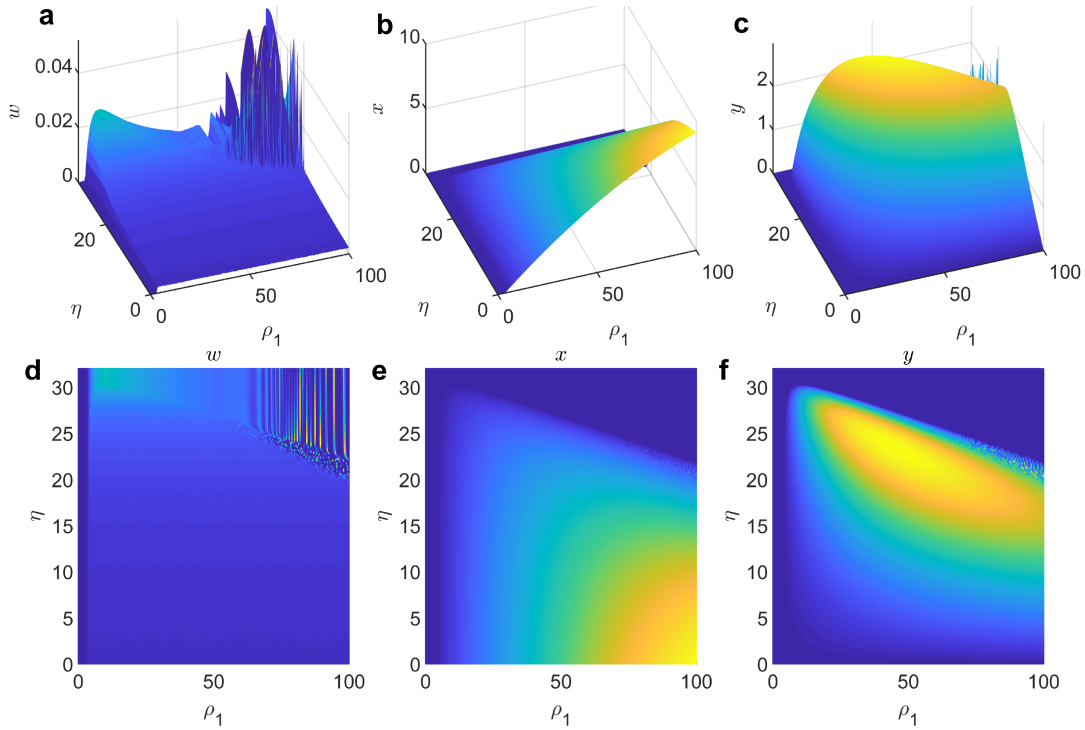

Figure 7: Equilibrium distribution of w,x and y vs. (ρ_1,η). (a)-(c) Equilibrium distribution of infected cells (w), CD8$^+$ T cells (x) and exhausted CD8$^+$ T cells (y), respectively. (d)-(f) The contour of (a)-(c), respectively.

(i) Below $\eta^{c_1}=22.9840$ (where $\phi_3(\eta)=0$), the immune-controlled state S_3 remains LAS (see Fig. 8 with $\eta=20$).

(ii) For $\eta\in(\eta^{c_1},\eta^{c_3})=(22.9840,23.9894)$, periodic solutions emerge via Hopf bifurcation, with oscillation amplitudes of $u(t)$, $w(t)$ and $v(t)$ growing gradually while CD8$^+$ T cell populations ($x(t)$ and $y(x)$) diminish rapidly following the increase of η (see Fig. 8 with $\eta=25$ and $\eta=26$).

(iii) Beyond $\eta^{c_3}=23.9894$, the immune cell oscillations vanish completely, leaving only infected cell dynamics (see Fig. 8 with $\eta=26$). These phase-dependent amplitude modulations demonstrate how T cell exhaustion progressively decouples immune responses from viral replication.

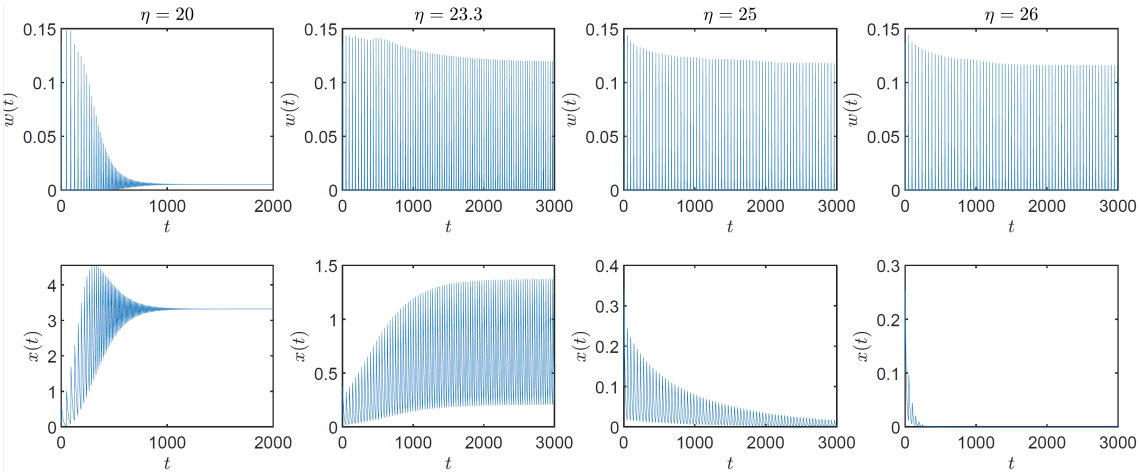

Figure 8: Time evolution of $w(t)$ and $x(t)$. Time evolution of infected cells ($w(t)$) and CD8$^+$ T cells ($x(t)$) under different exhaustion rates $\eta=20,23.3,25,26$. Here, $\rho_1=80$.

4 Conclusion and discussion

CD8$^+$ T cells play a pivotal role in adaptive immunity by mediating cytotoxic clearance of virus-infected cells. To maintain effective antiviral functions, these cells must preserve specific functional profiles through controlled differentiation from naive to effector and ultimately memory states, a process accompanied by dynamic metabolic reprogramming to meet stage-specific energy demands [12,14]. However, during chronic viral infections, persistent antigen exposure drives CD8$^+$ T cells into an exhausted state characterized by progressive functional impairment [11,26]: hierarchical loss of cytokine production, diminished cytotoxic capacity, and eventual failure to control viral replication. As exhaustion propagates through the T cell population, pathogen clearance becomes increasingly compromised.

In this paper, we explored the effects of CD8$^+$ T cells exhaustion on the viral dynamics, by mathematical modeling. We consider within-host viral infection with two transmission modes, virus-to-cell and cell-to-cell transmissions, and logistic target cell growth. Additionally, we accounted for the CD8$^+$ T cells (including stem-like progenetor/precursor and effector-like transitory T_{ex}) and terminally exhausted CD8$^+$ T cells. We established the nonnegativity and boundedness of the solutions, and identified the existence of three non-trivial equilibria: infection-free $S_1=(1,0,0,0,0)$, uncontrolled-infection $S_2=(\bar{u},\bar{w},\bar{v},0,0)$, and immune-established $S_3=(\hat{u},\hat{w},\hat{v},\hat{x},\hat{y})$. The local asymptotic stability of these equilibria are partly governed by the basic reproductive number $\mathcal{R}_0$ and the immune response related threshold $\mathcal{R}_1$:

(i) S_1 is LAS for $\mathcal{R}_0<1$.

(ii) S_2 is LAS for $\mathcal{R}_0>1$ and $\mathcal{R}_1>1$ with an additional condition $\phi_1(p)>0$.

(iii) S_3 is LAS for $\mathcal{R}_0>1$ and $\mathcal{R}_1>1$ with additional conditions $\phi_2(p)>0$ and $\phi_3(p)>0$.

The global stability of S_1 and S_2 are also presented. The system experiences transcritical bifurcations at S_1 and S_2 as a bifurcation parameter passes the critical values satisfying $\mathcal{R}_0(p)=1$ and $\mathcal{R}_1(p)=1$, and lose its stability to S_2 and S_3, respectively. The system also exhibits Hopf bifurcations at S_2 and S_3 as a bifurcation parameter crosses the critical values with $\phi_1(p)=0$ and $\phi_3(p)=0$, and periodic solutions bifurcate from S_2 and S_3, respectively. Setting ρ_1 as a bifurcation parameter, the numerical simulation shows the full spectrum of bifurcation dynamics of the system under low exhaustion rate and high exhaustion rate, respectively (see Figs. 2-5).

Numerical bifurcation analysis with respect to infection rate (ρ_1) and exhaustion rate (η) revealed four dynamical regimes governing viral persistence:

(i) "High exhaustion rate" leads to failed immune containment, with either stable high viral loads (homogeneous) or sustained oscillations.

(ii) "Intermediate exhaustion rate + low infection rate" generates exhaustion-dominated CD8$^+$ T populations and progressive infection spread.

(iii) "Intermediate exhaustion rate + high infection rate" causes immune collapse and oscillatory infection persistence.

(iv) "Low exhaustion rate" enables durable CD8$^+$ T cell-mediated control, suppressing infection to very low levels (see Figs. 6-7).

To explore the role of T cell exhaustion in chronic viral infections, we developed a simplified mathematical model that intentionally focuses on core dynamics. While this approach provides analytical tractability, several limitations should be noted:

(i) We aggregated diverse CD8$^+$ T cell states (e.g. stem-like, effector-like subsets) into a single exhausted population, neglecting subtype-specific dynamics [26].

(ii) The model also ignores tissue compartmentalization and spatial immune-viral interactions that may influence exhaustion kinetics.

(iii) The parameters governing exhaustion kinetics lack direct experimental validation due to scarce longitudinal data on PD-1^+ $CD8^+$ T cell dynamics in HIV progression, making our results primarily theoretical.

(iv) While the model generates high-frequency periodic solutions, these fail to fully capture clinical phenomena like viral blips, suggesting unresolved biological complexity in feedback regulation.

Future work with experimental datasets will enable parameter estimation and model validation. Nevertheless, our current mathematical analysis and numerical simulations offer novel insights into how exhaustion shapes within-host viral dynamics, particularly in establishing conditions for viral persistence versus immune control.

Acknowledgment

X. Lai is partially supported by the National Natural Science Foundation of China (Grant Nos. 12171478, 12331018).

References

[1] A. E. S. Almocera, V. K. Nguyen, and E. A. Hernández-Vargas, *Multiscale model within-host and between-host for viral infectious diseases*, J. Math. Biol., 77(4):1035–1057, 2018.

[2] A. Alrubayyi, E. Moreno-Cubero, D. Hameiri-Bowen, R. Matthews, S. Rowland-Jones, A. Schurich, and D. Peppa, *Functional restoration of exhausted CD8 T cells in chronic HIV-1 infection by targeting mitochondrial dysfunction*, Front. Immunol., 13:908697, 2022.

[3] A. Barbehenn et al., *Rapid biphasic decay of intact and defective HIV DNA reservoir during acute treated HIV disease*, Nat. Commun., 15:9966, 2024.

[4] J.-C. Beltra et al., *Developmental relationships of four exhausted CD8+ T cell subsets reveals underlying transcriptional and epigenetic landscape control mechanisms*, Immunity, 52(5):825–841, 2020.

[5] S. Bonhoeffer, R. M. May, G. M. Shan, and M. A. Nowak, *Virus dynamics and drug therapy*, Proc. Natl. Acad. Sci. USA, 94(13):6971–6976, 1997.

[6] M. Ciupe, B. Bivort, D. Bortz, and P. Nelson, *Estimating kinetic parameters from HIV primary infection data through the eyes of three different mathematical models*, Math. Biosci., 200(1):1–27, 2006.

[7] H. Dahari, A. Lo, R. M. Ribeiro, and S. Perelson, *Modeling hepatitis C virus dynamics: Liver regeneration and critical drug efficacy*, J. Theor. Biol., 247(2):371–381, 2007.

[8] M. P. Davenport, R. M. Ribeiro, L. Zhang, D. P. Wilson, and A. S. Perelson, *Understanding the mechanisms and limitations of immune control of HIV*, Immunol. Rev., 216:164–175, 2007.

[9] L. Galluzzi, K. N. Smith, A. Liston, and A. D. Garg, *The diversity of $CD8^+$ T cell dysfunction in cancer and viral infection*, Nat. Rev. Immunol., 25:662–679, 2025.

[10] T. Guo, Z. Qiu, M. Shen, J. Li, and Y. Chen, *Dynamics of a new HIV model with the activation status of infected cells*, J. Math. Biol., 82(6):51, 2021.

[11] C. Fenwick, V. Joo, P. Jacquier, A. Noto, R. Banga, M. Perreau, and G. Pantaleo, *T-cell exhaustion in HIV infection*, Immunol. Rev., 292(1):149–163, 2019.

[12] J. T. Harty, A. R. Tvinnereim, and D. W. White, *CD8+ T cell effector mechanisms in resistance to infection*, Annu. Rev. Immunol., 18:275–308, 2000.
[13] S. C. Jameson and D. Masopust, *Diversity in T cell memory: An embarrassment of riches*, Immunity, 31(6):859–871, 2009.
[14] S. M. Kaech, E. J. Wherry, and R. Ahmed, *Effector and memory T-cell differentiation: Implications for vaccine development*, Nat. Rev. Immunol., 2:251–262, 2002.
[15] T. Kajiwara, T. Sasaki, and Y. Takeuchi, *Construction of Lyapunov functionals for delay differential equations in virology and epidemiology*, Nonlinear Anal. Real World Appl., 13(4):1802–1826, 2012.
[16] J. Kennedy and R. Eberhart, *Particle swarm optimization*, in: Proceedings of the IEEE International Conference on Neural Networks, Vol. 4, IEEE, 1942–1948, 1995.
[17] N. L. Komarova, D. Anghelina, I. Voznesensky, B. Trinité, D. N. Levy, and D. Wodarz, *Relative contribution of free-virus and synaptic transmission to the spread of HIV-1 through target cell populations*, Biol. Lett., 9(1):20121049, 2013.
[18] A. Korobeinikov, *Global properties of basic virus dynamics models*, Bull. Math. Biol., 66:879–883, 2004.
[19] X. Lai and X. Zou, *Modeling HIV-1 virus dynamics with both virus-to-cell infection and cell-to-cell transmission*, SIAM J. Appl. Math., 74(3):898–917, 2014.
[20] X. Lai and X. Zou, *Modeling cell-to-cell spread of HIV-1 with logistic target cell growth*, J. Math. Anal. Appl., 426:898–917, 2015.
[21] J. P. LaSalle, *The Stability of Dynamical Systems*, in: CBMS-NSF Regional Conference Series in Applied Mathematics, Vol. 25, SIAM, 1976.
[22] J. Li, X. Huo, and Y. Chen, *Threshold dynamics of a viral infection model with defectively infected cells*, Math. Biosci. Eng., 19:6489–6503, 2022.
[23] J. Li, Y. Xiao, F. Zhang, and Y. Yang, *An algebraic approach to proving the global stability of a class of epidemic models*, Nonlinear Anal. Real World Appl., 13(5):2006–2016, 2012.
[24] S. Marino, I. B. Hogue, C. J. Ray, and D. E. Kirschner, *A methodology for performing global uncertainty and sensitivity analysis in systems biology*, J. Theor. Biol., 254(1):178–196, 2008.
[25] M. Markowitz, M. Louie, A. Hurley, E. Sun, M. D. Mascio, A. S. Perelson, and D. D. Ho, *A novel antiviral intervention results in more accurate assessment of human immunodeficiency virus type 1 replication dynamics and T-cell decay in vivo*, J. Virol., 77(8):5037–5038, 2003.
[26] L. M. McLane, M. S. Abdel-Hakeem, and E. J. Wherry, *CD8 T cell exhaustion during chronic viral infection and cancer*, Annu. Rev. Immunol., 37:457–495, 2019.
[27] A. S. Perelson and P. W. Nelson, *Mathematical analysis of HIV-1 dynamics in vivo*, SIAM Rev., 41(1):3–44, 1999.
[28] L. Perko, *Differential Equations and Dynamical Systems*, Springer, 2001.
[29] D. R. Sen et al., *The epigenetic landscape of T cell exhaustion*, Science, 354(6316):1165–1169, 2016.
[30] A. H. Sharpe and K. E. Pauken, *The diverse functions of the PD1 inhibitory pathway*, Nat. Rev. Immunol., 18(3):153–167, 2018.
[31] M. Shen, Y. Xiao, L. Rong, and L. A. Meyers, *Conflict and accord of optimal treatment strategies for HIV infection within and between hosts*, Math. Biosci., 309:107–117, 2019.
[32] H. Shu, Y. Chen, and L. Wang, *Impacts of the cell-free and cell-to-cell infection modes on viral dynamics*, J. Dynam. Differential Equations, 30(4):1817–1836, 2018.
[33] A. Tsegaye et al., *Stable pattern of HIV-1 subtype C Gag-specific T-cell responses coincides with slow rate of CD4 T-cell decline in HIV-infected Ethiopians*, AIDS, 21(3):369–372, 2007.
[34] M. Tsiang, J. F. Rooney, J. J. Toole, and C. S. Gibbs, *Biphasic clearance kinetics of hepatitis B virus from patients during adefovir dipivoxil therapy*, Hepatology, 29(6):1863–1869, 1999.

[35] A. Wang and M. Y. Li, *Viral dynamics of HIV-1 with CTL immune response*, Discrete Contin. Dyn. Syst. Ser. B, 26(4):2257–2272, 2021.
[36] S. Wang, Q. Zhang, H. Hui, K. Agrawal, M. A. Y. Karris, and T. M. Rana, *An atlas of immune cell exhaustion in HIV-infected individuals revealed by single-cell transcriptomics*, Emerg. Microbes Infect., 9(1):2333–2347, 2020.
[37] Y. Wang, J. Liu, X. Zhang, and J. M. Heffernan, *An HIV stochastic model with cell-to-cell infection, B-cell immune response and distributed delay*, J. Math. Biol., 86(3):35, 2023.
[38] Y. Wang, Y. Zhou, F. Brauer, and J. M. Heffernan, *Viral dynamics model with CTL immune response incorporating antiretroviral therapy*, J. Math. Biol., 67(5):901–934, 2013.
[39] E. J. Wherry et al., *Molecular signature of CD8+ T cell exhaustion during chronic viral infection*, Immunity, 35(4):375–387, 2011.
[40] E. J. Wherry and M. Kurachi, *Molecular and cellular insights into T cell exhaustion*, Nat. Rev. Immunol., 15(8):486–499, 2015.
[41] D. Wodarz and M. A. Nowak, *Specific therapy regimes could lead to long-term immunological control of HIV*, Proc. Natl. Acad. Sci. USA, 96(25):14464–14469, 1999.
[42] P. Yu, *Closed-form conditions of bifurcation points for general differential equations*, Int. J. Bifurc. Chaos, 15(04):1467–1483, 2005.
[43] F. Zhang, J. Li, C. Zheng, and L. Wang, *Dynamics of an HBV/HCV infection model with intracellular delay and cell proliferation*, Commun. Nonlinear Sci. Numer. Simul., 42:464–476, 2017.